©Copyright 2013
Jake D. Quenzer

# Observability Based Path Planning in Range-only Localization

Jake D. Quenzer

A thesis submitted in partial fulfillment of the requirements for the degree of

Master of Science in Aeronautics & Astronautics

University of Washington

2013

Reading Committee:

Kristi A. Morgansen, Chair

Juris Vagners

Program Authorized to Offer Degree:
William E. Boeing Department of Aeronautics and Astronautics

University of Washington

**Abstract**

Observability Based Path Planning in Range-only Localization

Jake D. Quenzer

Chair of the Supervisory Committee:
Associate Professor Kristi A. Morgansen
William E. Boeing Department of Aeronautics and Astronautics

The motivations of oceanographic research have driven the development of autonomous underwater vehicles (AUVs) now capable of great feats of autonomy and endurance. It is anticipated that the future of autonomous oceanographic surveys will be conducted with mixed teams of vehicles that will reduce cost and improve data quality. In a commonly proposed scenario, a scientific survey is carried out by a group of low-cost, simplistic AUVs while a more capable vehicle tends to the group; providing communication and navigation assistance. The goal of this thesis is to explore path planning methods for the aid vehicle that aim to improve localization performance experienced by survey vehicles. The two planning methods proposed make use of local observability measures to decide an aid vehicle's steering control. Simulations are conducted to test both methods against typical survey missions to investigate their efficacy in improving localization performance.

# TABLE OF CONTENTS

# LIST OF FIGURES

# ACKNOWLEDGMENTS

The author wishes to express sincere appreciation to his adviser Kristi Morgansen for her time and guidance. Also, his thanks go out to Nathan, Brian, Caleb, and Atiye for their assistance and advice during the creation of this thesis. Finally, the author wishes to express great appreciation to his wife, Kamille, for her support, encouragement, and sacrifice during the making of this thesis, graduate school, and throughout our lives together.

# Chapter 1

# INTRODUCTION

## *1.1 Motivation*

In 1989 Henry Stommel, a respected physical oceanographer, envisioned [1] within the next decade a global ocean monitoring system consisting of a fleet of Autonomous Underwater Vehicles (AUVs) would provide long-term, large-scale oceanographic sampling to the world's oceanographers. Unfortunately, time has shown that his vision was overly ambitious in the performance, pervasiveness, and era of the imagined AUV fleet. Nonetheless, in the last decade we have indeed come to see a generation of AUVs, such as the University of Washington's Seaglider [2], that are capable of enduring many months and traversing thousands of kilometers with only periodic remote interaction. This generation of AUVs has been developed expediently to achieve a prevalence of autonomous *vehicles*. Given the complexity, size, and temporal scale of ocean dynamics meant to be studied with AUVs, we anticipate that further oceanographic research will stand to benefit from studies conducted by autonomous *systems* that are yet to be realized.

A modern vision [3] for the future of autonomous ocean sampling was provided by researchers at the Woods Hole Oceanographic Institution (WHOI) in 2012. In the vision, it is observed that present sampling methods require, at great monetary cost, a manned research vessel to deploy, command, track, re-supply, and capture robotic sampling vehicles. The researchers imagine a team of mixed-ability vehicles that could preclude the need for a manned vessel in all its previous roles, save deployment and recovery of the team. The vision is presented as three stages of progression from present methods and vehicles to the completely autonomous team of the final stage.

While the final stage of the vision is currently impractical, the intermediate notions frame pertinent goals in modern AUV system capability.

The first stage of the vision employs an advanced AUV to tend a small group of survey vehicles performing operations over a relatively small survey area (10 to 100 square meters) for a matter of hours or possibly days. According to the authors [3], the first stage of the vision is nearly achievable with current technology and they present a prototype of a representative system. Moving ahead, the second stage focuses on a class of missions referred to as ridge-segment scale; corresponding to surveys that span many kilometers over weeks or months. In these missions the survey vehicles are envisioned as low-cost underwater gliders and the tending vehicle is either an autonomous surface vehicle (ASV) or an advanced AUV. The autonomy and cooperation required to allow long term operation of otherwise under-equipped survey vehicles presents an overarching goal under which this work resides.

### *1.2 Problem Formulation*

In general, the model of operation proposed in the second stage of the WHOI vision proposes to use many relatively simple AUVs to perform a scientific survey while a more sophisticated vehicle tends to the group in place of a manned vessel. In work [4] that considers a similar scenario, the tending vehicle is dubbed a Communication and Navigation Aid (CNA). As the name suggests, the role of the CNA is to provide a relay for data transmission as well as a means of localization for the AUVs. Given a CNA is tasked with serving the communication and localization needs of a group of AUVs, a natural inquiry is how the CNA should navigate in order to best fulfill its duties. To more accurately couch the question, we consider further the CNA's two roles in the operational model:

**Communication** Communication between underwater vehicles over a ridge-segment scale distance is accomplished using an acoustic modem and transponder, like

the WHOI Micro-Modem [5]. Acoustic communication quality is well described by three factors:

- Throughput, the amount of information transmitted over a period of time, is largely affected by the frequency of the acoustic signal and processing capability of an acoustic modem. Higher frequency acoustic signals are more dramatically attenuated underwater. A CNA path aimed to increase throughput would minimize distance between vehicles to permit the use of higher frequency signals.
- Loss, the tendency for a transmission to be corrupted, is affected by a variety of factors including multipath propagation interference, environmental interference, and transducer directionality. The variety and complexity of these factors preclude a simple loss model; a CNA path designed to reduce loss would most likely implement a set of heuristically determined constraints on vehicle locations and depths.
- Latency, the duration between the production and reception of a transmission, is primarily affected by the distance between vehicles. A CNA path aimed to decrease latency would minimize distance between vehicles.

**Navigation** Navigation strategies for underwater vehicles generally depend on the locale of operation. Vehicles that operate near the water's surface often pair frequent GPS measurements with on-board inertial sensors. Alternatively, vehicles that operate mainly near the water's bottom often use Doppler Velocity Logs (DLVs) to track their position and velocity. Without assuming a specific role for the AUVs that would dictate proximity to the surface or bottom, acoustic localization provides a more generally applicable means of localization for AUVs.

When it comes to acoustic localization, there are a variety of practiced meth-

ods developed for various operational scenarios. Appendix A describes some of the relevant methods in further detail, but in essence an acoustic localization method produces a position estimate from range measurements to known locations. In most localization methods, the AUVs perform some form of estimation technique to incorporate on-board sensor measurements with acoustic range measurements. In order to increase an AUV's estimation performance, a CNA should move in such a way that an AUV's estimation problem is better conditioned, *i.e.* has a reduced sensitivity to the initial state of the system.

To summarize, we can improve communication quality for the most part by simply encouraging a small separation between vehicles, and we can improve navigation assistance by supporting a well conditioned estimation problem for each AUV. Because the separation requirement is straightforward, the goal of this thesis is to study the use of observability measures in the generation of a CNA path aimed at improving an AUV's localization performance.

### *1.3 Previous Work*

The CNA/AUV scenario at hand, withholding the communication motivation, has been the subject of much previous work under the title of Single Beacon Navigation (SBN). The typical scenario in SBN is flipped in the sense that an acoustic beacon is of known location/trajectory and an AUV path is planned or analyzed for its localization performance. An obvious drawback of planning an AUV path for localization is that the path cannot then be crafted to suit the needs of a survey or experiment.

A few, mostly earlier, works [6, 7, 8, 9] have been dedicated to the application and testing of estimation schemes for the single beacon navigation system. The estimation schemes implemented are Extended Kalman Filters (EKFs) and particle filters where EKFs are more predominant due to lower computational demand. These works omit an observability analysis but still obtain agreeable estimation performance

for "typical" AUV mission paths and provide compelling evidence for the benefit and practicality of the CNA/AUV mode of operation.

A variety of works have carried out observability analysis in the SBN system. Among them, a large group [10, 11, 12, 13] approximate the nonlinear system as a linear, time-varying (LTV) system and proceed to examine case-wise scenarios that degrade the linear system observability. Depending on the model used (inclusion of currents, moving beacon, etc.) the general result is that straight-line motions of the AUV that pass through the location of the beacon degrade observability. In other approaches [14, 15], the observability analysis is carried out on the original nonlinear system. The results of these works provide less restrictive constraints on the motions of the AUV. One work [14] derives a measure of observability specific to the system that provides some intuition regarding more or less observable trajectories for the AUV. Unfortunately, the observability measure was not explicitly used to systematically generate a AUV path for the experiments that concluded the work.

Toward the goal of determining optimal CNA trajectories there have been a handful of previous works. Most of these works generate a CNA path by [16, 17] employing the concept of maximum information gain, a concept often applied in the context of Simultaneous Localization and Mapping (SLAM). Essentially, the idea is to choose a CNA heading at each instant so as to increase the accuracy of every AUV's position estimate. In most cases the CNA does not have access to the AUV's real position estimate, so a model is used to allow the CNA to estimate the accuracy of each AUV's position estimate. Later work [18] uses a neural network structure that effectively learns what CNA actions result in increased AUV position accuracy. In comparison, there has been little work in generating a CNA path using observability measures at the core. In the case of an SBN scenario in a uniform flow, an analytic solution has been determined based on the LTV system and associated observability measures [11].

### *1.4 Contributions*

We present two methods of CNA path planning that approximately optimize the estimation condition number, an observability measure of the system that relates to how well conditioned the AUV's estimation problem is. The first method assumes an indefinite future trajectory and relates geometric properties of that trajectory to the estimation condition number. The second method simulates future trajectories for a finite time and relates the subsequent predicted measurements to the estimation condition number. In both methods, the control that yields the minimum estimation condition number is selected. Following the development of the decision processes, we investigate the traits of the paths they generate through a number of simulations. Finally, some common test scenarios are performed to demonstrate the potential of the decision methods to improve AUV localization performance.

### *1.5 Thesis Organization*

In Chapter 2, we discuss some background in acoustic localization and the CNA/AUV operational model as well as some background in system observability and observability measures. In Chapter 3, we develop the model and analysis that lead to a decision policy based on geometric properties of an assumed indefinite trajectory. In Chapter 4, we develop a separate model and analysis that lead to a decision policy based on predicted measurements that result from finite, simulated trajectories. In Chapter 5, we present path generation examples for both methods and simulate localization performance for a typical AUV mission. Finally, Chapter 6 contains concluding remarks as well as future work encouraged by this effort.

# Chapter 2

# BACKGROUND AND MATHEMATICAL PRELIMINARIES

Before developing any decision methods, we take this chapter to present some terminology and conceptual material which is applicable to the remainder. A complete presentation of linear systems theory can be found in [19]. A more complete context observability measures can be found in [20].

## *2.1 Observability*

The ability of an AUV to localize itself is tightly coupled with the concept of observability. There are notions of observability for both linear and nonlinear systems. Although the systems to be considered are nonlinear, they will be approximated as linear time varying. We will be concerned with the local observability of the linearized system and so only linear observability will be addressed here.

### *2.1.1 Observability Gramian*

Consider a linear system

$$\begin{aligned} \dot{\boldsymbol{x}} &= \boldsymbol{A}\boldsymbol{x} \\ \boldsymbol{y} &= \boldsymbol{C}\boldsymbol{x}, \end{aligned} \tag{2.1}$$

where $\boldsymbol{x} \in \mathcal{R}^n$, and $\boldsymbol{y} \in \mathcal{R}^m$. The state of the system at time $t$ is

$$\boldsymbol{x}(t) = e^{\boldsymbol{A}t}\boldsymbol{x}(0), \tag{2.2}$$

and a measurement made at time $t$ is

$$\boldsymbol{y}(t) = \boldsymbol{C}e^{\boldsymbol{A}t}\boldsymbol{x}(0). \tag{2.3}$$

The system is said to be observable if, for any unknown initial state $\boldsymbol{x}(0)$, there exists a finite $t_1 > 0$ such that the knowledge of the output over the interval $[0\ t_1]$ is sufficient to uniquely determine $\boldsymbol{x}(0)$ [19]. The local observability gramian of a system is an $n \times n$ matrix defined as

$$\boldsymbol{P}(t) = \int_0^t e^{\boldsymbol{A}'\tau} \boldsymbol{C}' \boldsymbol{C} e^{\boldsymbol{A}\tau} d\tau. \tag{2.4}$$

If the local observability gramian is nonsingular for any $t > 0$, the system is observable. The proof of this relationship is reproduced here from [19] because of its importance in the remainder.

**Theorem 1.** *The state equation (2.1) is observable if and only if the local observability gramian is nonsingular for any $t > 0$.*

*Proof.* We premultiply (2.3) by $e^{\boldsymbol{A}'t}\boldsymbol{C}'$ and then integrate it over $[0\ t_1]$ to yield

$$\left( \int_0^{t_1} e^{\boldsymbol{A}'t} \boldsymbol{C}' \boldsymbol{C} e^{\boldsymbol{A}t} dt \right) \boldsymbol{x}(0) = \int_0^{t_1} e^{\boldsymbol{A}'t} \boldsymbol{C}' \boldsymbol{y}(t) dt. \tag{2.5}$$

If $\boldsymbol{P}(t_1)$ is nonsingular, then

$$\boldsymbol{x}(0) = \boldsymbol{P}^{-1}(t_1) \int_0^{t_1} e^{\boldsymbol{A}'t} \boldsymbol{C}' \boldsymbol{y}(t) dt. \tag{2.6}$$

This yields a unique $\boldsymbol{x}(0)$. This shows that if $\boldsymbol{P}(t)$, for any $t > 0$, is nonsingular, then (2.1) is observable. Next we show that if $\boldsymbol{P}(t_1)$ is singular or, equivalently, positive semidefinite for all $t_1$, then (2.1) is not observable. If $\boldsymbol{P}(t_1)$ is positive semidefinite, there exists an $n \times 1$ nonzero constant vector $\boldsymbol{v}$ such that

$$\begin{aligned} \boldsymbol{v}' \boldsymbol{P}(t_1) \boldsymbol{v} &= \int_0^{t_1} \boldsymbol{v}' e^{\boldsymbol{A}'\tau} \boldsymbol{C}' \boldsymbol{C} e^{\boldsymbol{A}\tau} \boldsymbol{v} d\tau \\ &= \int_0^{t_1} \| \boldsymbol{C} e^{\boldsymbol{A}\tau} \boldsymbol{v} \|^2 d\tau = 0, \end{aligned} \tag{2.7}$$

which implies

$$\boldsymbol{C} e^{\boldsymbol{A}\tau} \boldsymbol{v} \equiv \boldsymbol{0}. \tag{2.8}$$

for all $t$ in $[0\ t_1]$. If $\boldsymbol{u} \equiv \boldsymbol{0}$, then $\boldsymbol{x}_1(0) = \boldsymbol{v} \neq \boldsymbol{0}$ and $\boldsymbol{x}_2(0) = \boldsymbol{0}$ both yield the same $\boldsymbol{y}(t) = \boldsymbol{C} e^{\boldsymbol{A}t} \boldsymbol{x}_i(0) \equiv \boldsymbol{0}$. Two different initial states yield the same zero-input response; therefore we cannot uniquely determine $\boldsymbol{x}(0)$. Thus (2.1) is not observable. □

### *2.1.2 Empirical Observabitily Gramian*

In many systems the local observability gramian can be difficult or intractable to calculate. In [20], an approximation to the gramian is given as the empirical local observability gramian. To define the empirical gramian, consider an initial state of the system $\boldsymbol{x}^0$ and a small displacement of length $\epsilon$. Let $\boldsymbol{x}^{\pm i} = \boldsymbol{x}^0 \pm \epsilon \boldsymbol{e}^i$ be a perturbed initial state where $\boldsymbol{e}$ is a unit vector in $\mathcal{R}^n$ to indicate the direction of the perturbation. The corresponding output of a system having a perturbed initial state is represented as $\boldsymbol{y}^{\pm i}(t)$. The empirical local observability gramian $\hat{\boldsymbol{P}}(T, \boldsymbol{x}^0)$ is an $n \times n$ matrix with $(i, j)$ component defined

$$\hat{\boldsymbol{P}}(T, \boldsymbol{x}^0)_{i,j} = \frac{1}{4\epsilon^2} \int_0^T (\boldsymbol{y}^{+i}(t) - \boldsymbol{y}^{-i}(t))'(\boldsymbol{y}^{+j}(t) - \boldsymbol{y}^{-j}(t))dt. \tag{2.9}$$

For a smooth system, the empirical gramian converges to the local observability gramian as $\epsilon \to 0$.

### *2.1.3 Observability Metrics*

The rank of the observability gramian provides a binary test of a system's observability. In [20], the authors examine the relationship between a system's observability characteristics and any associated estimation scheme. From that analysis they propose two measures relating estimation accuracy to system observability. The first is called the local unobservability index and is defined as the reciprocal of the smallest singular value of the observability gramian. The index is explained to be a measure of how large an effect observation noise can have on estimation error. The second measure is called the local estimation condition number, defined as the ratio of the largest to smallest singular values of the observability gramian. The condition number is explained to be a measure of how a small perturbation in the system's initial state in a given direction can dominate the output observed in a different state direction. As suggested by the choice of name, a large estimation condition number implies that

any estimation scheme aimed at inverting the map of states to measurements will be ill conditioned.

## *2.2 Localization*

In the exposition of the next chapters, the observation equations of the considered systems will have a large bearing on the derivation of the to-be-determined decision methods. The terms of these observation equations are dependent on the assumptions of the localization scheme employed. Here we discuss some such assumptions that are consistent with most or all of the acoustic localization methods described in Appendix A.

Given an AUV/CNA pair as depicted in Fig. 2.1, we can easily assume the CNA is capable of obtaining a GPS measurement of its own absolute position. We can be almost certain that any AUV which operates without a tether will be capable of sensing its depth to a high degree of accuracy. In any form of acoustic localization an AUV will necessarily measure the distance between itself and a beacon/CNA. To measure that distance the AUV can sent an acoustic ping to a beacon/CNA to which the beacon/CNA will automatically issue a reply. In this scheme the One Way Travel Time (OWTT) of the ping can be determined by measuring the flight time of the message and incorporating *a priori* knowledge of the time required for the beacon/CNA to process the ping and issue a response (the delay attributed to processing time is often called Turn Around Time or TAT),

$$t_{OWTT} = \frac{t_{flight} - t_{TAT}}{2}. \tag{2.10}$$

The slant range between the vehicle to the beacon/CNA can then be calculated using a depth-average speed of sound in water, $c$, and the OWTT,

$$r_s = c \times t_{OWTT}. \tag{2.11}$$

In a different range measurement scheme, the beacon/CNA will simply transmit pings at exact points in time. An AUV with a well synchronized clock will then be able

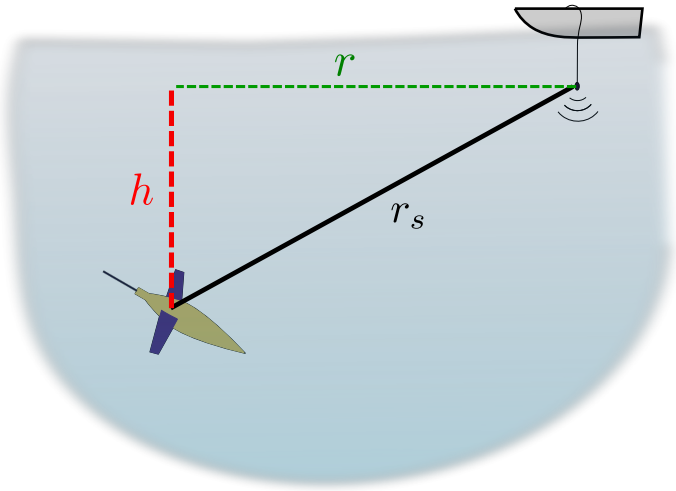


Figure 2.1: A typical AUV/CNA geometry: The AUV is an underwater vehicle at depth $h$, whereas the CNA is a surface vehicle. The vehicles are separated in three dimensions by a slant range, $r_s$, and in two dimensions by their planar separation, $r$.

to determine the OWTT by simply subtracting the known transmission time from the time of arrival. Given the AUV has methods to measure $h$ and $r_s$ as labeled in Fig. 2.1, we see that the planar range, $r$ can be directly calculated. Thus, in most constructions of acoustic localization schemes it is the surface-planar position of the AUV which is of interest.

Another key assumption in the measurements obtainable by an AUV is the transmission of CNA state to the team of AUVs. As depicted in Fig. 2.1, the location of the CNA may vary in time. The low bandwidth of acoustic communication prevents all-to-all communication of full state information, however it is commonly assumed that the beacon/CNA in an acoustic localization scheme will transmit its state either when it receives a ping or following a scheduled transmission, depending on the scheme implemented. Thus, we can generally assume that an AUV will have knowledge of the position, speed, and direction of travel of a mobile beacon/CNA.

# Chapter 3

# PATH INERTIA METHOD

Having established the relevant background, the topic of this chapter will be to determine a CNA steering control scheme that is based on the relationship between predicted path geometry and the local estimation condition number. The inspiration for this decision scheme comes from the results of a previous work [11]. As it was presented, the analysis in that work considered the path of an AUV about a fixed beacon. In what follows we will start by restating the analysis of [11] that draws a connection between path geometry and the estimation condition number. Next, we will show that the relationship observed can, in extension, be applied to the path of a CNA about an AUV. We will then present the control scheme in its basic form as well as modifications inspired by simulation results.

## *3.1 System Analysis*

### *3.1.1 Fixed CNA*

The development of the system dynamics and observability analysis of this section are reproduced from prior work [11], in order to introduce the ideas underpinning the control scheme. The CNA in this system is held fixed at the origin while a single

AUV is modeled with constant speed unicycle dynamics in a uniform flow field:

$$\begin{aligned}\dot{\boldsymbol{x}} &= \begin{bmatrix} x_3 \\ x_4 \\ 0 \\ 0 \end{bmatrix} + \begin{bmatrix} 1 \\ 0 \\ 0 \\ 0 \end{bmatrix} u_1 \begin{bmatrix} 0 \\ 1 \\ 0 \\ 0 \end{bmatrix} u_2 \\ \boldsymbol{u} &= \begin{bmatrix} V\cos(\psi) \\ V\sin(\psi) \end{bmatrix} \\ \boldsymbol{y} &= x_1^2 + x_2^2,\end{aligned} \tag{3.1}$$

where $\boldsymbol{x} = [x_E \ y_N \ W_x \ W_y]^T$ are the states, $u_1$ is a constrained East flow relative velocity, and $u_2$ is a constrained North flow relative velocity. The angle $\psi$ is the vehicle heading and is assumed to be directly measured.

We now linearize the system about an arbitrary trajectory. Let $(x_1^0(t), x_2^0(t), x_3^0(t), x_4^0(t))$ be the nominal trajectory. The linear dynamics are given by

$$\begin{aligned}\boldsymbol{A}(t) &= \begin{bmatrix} 0 & 0 & 1 & 0 \\ 0 & 0 & 0 & 1 \\ 0 & 0 & 0 & 0 \\ 0 & 0 & 0 & 0 \end{bmatrix} \\ \boldsymbol{C}(\boldsymbol{x}(t)) &= \begin{bmatrix} 2x_1^0(t) & 2x_2^0(t) & 0 & 0 \end{bmatrix}.\end{aligned} \tag{3.2}$$

The state transition matrix for the linear system is

$$\boldsymbol{\Phi}(t) = e^{\boldsymbol{A}t} = \begin{bmatrix} 1 & 0 & t & 0 \\ 0 & 1 & 0 & t \\ 0 & 0 & 1 & 0 \\ 0 & 0 & 0 & 1 \end{bmatrix}. \tag{3.3}$$

The local observability gramian for the linear system is computed to be

$$\boldsymbol{P}(T) = 4\int_0^T \begin{bmatrix} x_1^2 & x_1x_2 & tx_1^2 & tx_1x_2 \\ x_1x_2 & x_2^2 & tx_1x_2 & tx_2^2 \\ tx_1^2 & tx_1x_2 & t^2x_1^2 & t^2x_1x_2 \\ tx_1x_2 & tx_2^2 & t^2x_1x_2 & t^2x_2^2 \end{bmatrix} dt, \tag{3.4}$$

where the trajectory time dependence is dropped for brevity. It is observed that the entries of the gramian correspond to geometic properties of the trajectory. Specifically, $\boldsymbol{P}(T)$ can be represented as a block structure of inertia matrices

$$\boldsymbol{P}(T) = \begin{bmatrix} [I] & [I]_t \\ [I]_t & [I]_{t^2} \end{bmatrix}, \tag{3.5}$$

where

$$[I] = \begin{bmatrix} I_{x_2x_2} & I_{x_1x_2} \\ I_{x_1x_2} & I_{x_1x_1} \end{bmatrix} \tag{3.6}$$

is the inertia matrix of the trajectory of uniform unit mass. The $[I]_t$ and $[I]_{t^2}$ are trajectory inertia matrices with mass distribution $t$ and $t^2$ respectively. Under the assumption that the desire is for a trajectory that maximizes the observability of intertial information, only the first block of 3.5 need be considered. The eigenvalues of the first block are the principal moments of inertia of the trajectory. This relationship yields the conclusion that a trajectory with equal principal inertias will produce the lowest estimation condition number.

### *3.1.2 Fixed AUV*

In the scenario being considered for this thesis, the desire is to steer the CNA to improve an AUV's ability to localize itself relative to the CNA. The analysis of the previous section demonstrated a relationship between AUV path properties and the observability of the AUV's position relative to a static beacon. Consider now a similar analysis in which the AUV is fixed at the origin and the CNA is driven by unicycle

dynamics. Since the CNA is the agent with the "known" position, the AUV's goal is to localize itself relative to the CNA. Let us then consider the dynamics of the AUV relative to the CNA that result from the CNA's motion. Also, let us assume that there may be some difference in the uniform flow experienced by the AUV compared to that experienced by the CNA (for example, the vehicles operate at different depths and experience different currents). First, we define the relative state vector

$$\boldsymbol{r} = \begin{bmatrix} 0 \\ 0 \\ W_x + \Delta W_x \\ W_y + \Delta W_y \end{bmatrix} - \begin{bmatrix} x_E \\ y_N \\ W_x \\ W_y \end{bmatrix} = \begin{bmatrix} -x_1 \\ -x_2 \\ \Delta W_x \\ \Delta W_y \end{bmatrix}, \tag{3.7}$$

as the state of the AUV relative to the state of the CNA where the $\Delta$ terms account for the difference in the uniform flow experienced by the two vehicles. The relative state dynamics are

$$\begin{aligned} \dot{\boldsymbol{r}} &= \begin{bmatrix} -\dot{x}_1 + r_3 \\ -\dot{x}_2 + r_4 \\ 0 \\ 0 \end{bmatrix} \\ \boldsymbol{u} &= \begin{bmatrix} V\cos(\psi) \\ V\sin(\psi) \end{bmatrix} \\ y &= r_1^2 + r_2^2. \end{aligned} \tag{3.8}$$

Now, we can proceed to linearize the relative dynamics about an arbitrary relative trajectory. Using $(r_1^0(t), r_2^0(t), r_3^0(t), r_4^0(t))$ as the nominal trajectory, the linear dynamics

are given by

$$\boldsymbol{A}(t) = \begin{bmatrix} 0 & 0 & 1 & 0 \\ 0 & 0 & 0 & 1 \\ 0 & 0 & 0 & 0 \\ 0 & 0 & 0 & 0 \end{bmatrix} \tag{3.9}$$

$$\boldsymbol{C}(\boldsymbol{r}(t)) = \begin{bmatrix} 2r_1^0(t) & 2r_2^0(t) & 0 & 0 \end{bmatrix}.$$

The state transition matrix for this linear system is

$$\boldsymbol{\Phi}(t) = e^{\boldsymbol{A}t} = \begin{bmatrix} 1 & 0 & t & 0 \\ 0 & 1 & 0 & t \\ 0 & 0 & 1 & 0 \\ 0 & 0 & 0 & 1 \end{bmatrix}. \tag{3.10}$$

Finally, the observability gramian for this linear system is computed to be

$$\boldsymbol{P}(T) = 4\int_0^T \begin{bmatrix} r_1^2 & r_1 r_2 & t r_1^2 & t r_1 r_2 \\ r_1 r_2 & r_2^2 & t r_1 r_2 & t r_2^2 \\ t r_1^2 & t r_1 r_2 & t^2 r_1^2 & t^2 r_1 r_2 \\ t r_1 r_2 & t r_2^2 & t^2 r_1 r_2 & t^2 r_2^2 \end{bmatrix} dt. \tag{3.11}$$

Performing the substitutions $r_1 = -x_1$ and $r_2 = -x_2$ in (3.11) yields an equivalent observability gramian to that calculated in (3.4). We can conclude then that the systems (3.1) and (3.8) share identical observability traits. In what follows, we will exploit this equality to simplify the decision process.

### *3.2 Decision Process*

The basic goal of the method is to steer the CNA in a way that would minimize the estimation condition number if the CNA was localizing itself from a beacon located at the position of the AUV. Due to the relationship determined in the previous section, we then know that by solving this first problem we will simultaneously be solving the problem of determining a control for the CNA that will minimize the estimation

condition number of the relative position system. Minimizing this second condition number is how we increase the AUV's ability to localize itself with respect to the CNA.

As stated previously, there have been previous efforts to plan CNA paths in order to improve AUV localization performance. The majority of those works do not attempt to determine a globally optimal path either because the state space and decision space are continuous or because the relevant penalty functions are not mathematically amenable. The ideas of this chapter do not change those limitations, and so the decision method will be constructed as a locally optimal policy.

We start by approximating (3.1) with discrete dynamics

$$\begin{aligned} \boldsymbol{x}(n+1) &= \begin{bmatrix} x_1(n) \\ x_2(n) \\ x_3(n) \\ x_4(n) \end{bmatrix} + \begin{bmatrix} x_3(n)+u_1 \\ x_4(n)+u_2 \\ 0 \\ 0 \end{bmatrix} \delta t \\ \boldsymbol{u} &= \begin{bmatrix} V\cos(\psi) \\ V\sin(\psi) \end{bmatrix} \\ y &= x_1(n)^2 + x_2^2(n)^2. \end{aligned} \tag{3.12}$$

We seek a heading rate input that will minimize the condition number of the observability gramian based on a trajectory that would result if the heading rate were applied indefinitely. A constant heading rate $\dot{\psi}$ (deg/sec) corresponds to a circular trajectory where a positive turn rate yields a counter-clockwise motion. The circumference of the circular trajectory is

$$c = \frac{360}{\dot{\psi}} V, \tag{3.13}$$

which corresponds to a radius of

$$r = \frac{c}{2\pi} = \frac{360}{\dot{\psi} 2\pi} V. \tag{3.14}$$

The inertia matrix for the circular trajectory by itself is

$$\boldsymbol{I} = \begin{bmatrix} r^2/2 & 0 \\ 0 & r^2/2 \end{bmatrix}. \tag{3.15}$$

The parallel axis theorem can be used to determine the inertia of the trajectory relative to the origin

$$\boldsymbol{J} = \boldsymbol{I} + m(\hat{\boldsymbol{c}}^2\mathbf{1} - \hat{\boldsymbol{c}}\hat{\boldsymbol{c}}^T), \tag{3.16}$$

where $\hat{\boldsymbol{c}}$ is the location of the center of the circular trajectory

$$\hat{\boldsymbol{c}} = \begin{bmatrix} x_1(n) \\ x_2(n) \end{bmatrix} - r \begin{bmatrix} 0 & 1 \\ -1 & 0 \end{bmatrix} \begin{bmatrix} \cos(\psi) \\ \sin(\psi) \end{bmatrix}. \tag{3.17}$$

This gives an expression of $\boldsymbol{J}$ that can be written as

$$\boldsymbol{J} = \begin{bmatrix} r^2/2 & 0 \\ 0 & r^2/2 \end{bmatrix} + \begin{bmatrix} \hat{\boldsymbol{c}}^T\hat{\boldsymbol{c}} & 0 \\ 0 & \hat{\boldsymbol{c}}^T\hat{\boldsymbol{c}} \end{bmatrix} - \hat{\boldsymbol{c}}\hat{\boldsymbol{c}}^T, \tag{3.18}$$

which has eigenvalues

$$\begin{aligned} \lambda_1 &= \frac{3}{2}r^2 - 2\sin(\psi)rx_1(n) + 2\cos(\psi)rx_2(n) + x_1^2(n) + x_2^2(n) \\ \lambda_2 &= \frac{1}{2}r^2. \end{aligned} \tag{3.19}$$

In order to reduce the condition number of the observability gramian, we wish to make the eigenvalues of $\boldsymbol{J}$ equal. In other words, we wish to minimize the difference between the eigenvalues. The difference can be written simply as

$$\lambda_1 - \lambda_2 = r^2 - 2r\sin(\psi)x_1(n) + 2r\cos(\psi)x_2(n) + x_1(n)^2 + x_2(n)^2 \tag{3.20}$$

This expression is a quadratic in terms of $r$ which gives a convex minimization problem,

$$\underset{r}{\text{minimize}} \quad r^2 - 2r\sin(\psi)x_1(n) + 2r\cos(\psi)x_2(n) + x_1(n)^2 + x_2(n)^2. \tag{3.21}$$

Since the last two terms are constant at each time step, they can be removed without changing the solution:

$$\underset{r}{\text{minimize}} \quad r^2 - 2r\sin(\psi)x_1(n) + 2r\cos(\psi)x_2(n). \tag{3.22}$$

Notice that the solution may result in a turning radius that is smaller than the vehicle is capable of achieving. Instead of forcing the problem to be non-convex, we may further approximate by rounding a result to the nearest of the minimum positive or negative turning radius.

Through simulation we found that the method, as-is, tends to produce large distances between the CNA and AUVs. As a result, we add a penalty to the cost function that represents the distance between the vehicles. Future distances between the CNA and the AUV can be thought of as the addition of the distance from the AUV to the center of the circular trajectory plus some portion of the circle's radius. The center of the circular trajectory $\hat{\boldsymbol{c}}$ was defined in (3.17). If we let

$$c = \|\hat{\boldsymbol{c}}\|_2^2, \tag{3.23}$$

and we take the circular trajectory to have radius $r$, then we have the new problem

$$\underset{r}{\text{minimize}} \quad r^2 - 2r\sin(\psi)x_1(n) + 2r\cos(\psi)x_2(n) + \gamma(c + |r|), \tag{3.24}$$

where $\gamma$ is a positive constant that can be adjusted to emphasize the relative importance between minimal estimation condition number and future distance between the AUV and CNA.

Finally, toward the more general goal of a CNA tending a group of AUVs, we construct the decision process to handle multiple AUVs. In the previous description of the method the AUV was fixed at the origin of a global coordinate plane; there was no difference between the position of the CNA in the global coordinates and the position of the CNA relative to the AUV. The position of the CNA relative to the AUV is the actual position of interest, and so when considering multiple AUVs we

will work with an array of relative CNA positions

$$\begin{bmatrix} \breve{x}_{1_1} & \breve{x}_{1_2} & \dots & \breve{x}_{1_n} \\ \breve{x}_{2_1} & \breve{x}_{2_2} & \dots & \breve{x}_{2_n} \end{bmatrix}, \tag{3.25}$$

where $n$ is the number of AUVs. The decision process can be extended so that one optimization provides the turning angle that best satisfies the estimation condition number and separation costs incurred from each AUV. Given the array of relative CNA positions the cost function of the decision problem can be re-stated as,

$$\underset{r}{\text{minimize}} \quad \sum_{i=1}^{n} r^2 - 2r\sin(\psi)\breve{x}_{1_i} + 2r\cos(\psi)\breve{x}_{2_i} + \gamma(c_i + |r|), \tag{3.26}$$

where $c_i$ is calculated with (3.17) using the $i$-th relative coordinates.

# Chapter 4

# EMPIRICAL GRAMIAN METHOD

The system analysis for this method will proceed similarly to that for the previous method. First, we will consider system in which the CNA is fixed at the origin and the AUV is governed by constant speed unicycle dynamics. We will then consider a different system in which the AUV is fixed and the CNA behaves according to the previous dynamics. The motion of the AUV relative to the CNA will be evaluated for its similarity in observability traits to the original system. We will then be able to use the first system analysis for determining the CNA decision process.

## *4.1 System Analysis*

### *4.1.1 Fixed CNA*

Consider a system in which the CNA is fixed at the origin and the AUV is governed by constant speed unicycle dynamics

$$\begin{aligned} \dot{\boldsymbol{x}} &= \begin{bmatrix} V\cos(\psi) \\ V\sin(\psi) \\ 0 \end{bmatrix} + \begin{bmatrix} 0 \\ 0 \\ 1 \end{bmatrix} u \\ y &= \begin{bmatrix} \psi \\ x_1^2 + x_2^2 \end{bmatrix}, \end{aligned} \tag{4.1}$$

where the state vector is $x = [x_E \quad y_N \quad \psi]^T$ and the control is turning rate. In this setting, the heading angle is 0 in the $x_E$ direction and positive in a counter-clockwise direction. We can linearize (4.1) about an arbitrary nominal trajectory

$(x_1^0(t), x_2^0(t), x_3^0(t))$ to obtain

$$\begin{aligned} \boldsymbol{A}(t) &= \begin{bmatrix} 0 & 0 & 0 & -V\sin(\psi) \\ 0 & 0 & 0 & V\cos(\psi) \\ 0 & 0 & 0 & 0 \\ 0 & 0 & 0 & 0 \end{bmatrix} \\ \boldsymbol{C}(t) &= \begin{bmatrix} 0 & 0 & \psi \\ 2x_1^0 & 2x_2^0 & 0 \end{bmatrix}. \end{aligned} \tag{4.2}$$

If we could determine the state transition matrix we could then compute the observability gramian as

$$\boldsymbol{P}(T) = \int_0^T \boldsymbol{\Phi}'(t,t_0)\boldsymbol{C}'(t,t_0)\boldsymbol{C}(t,t_0)\boldsymbol{\Phi}(t,t_0)dt. \tag{4.3}$$

Because the state transition matrix is not readily determined for this system, we will instead approximate $\boldsymbol{P}(T)$ with the empirical observability gramian

$$\hat{\boldsymbol{P}}(T,\boldsymbol{x}^0) = \frac{1}{4\epsilon^2}\int_0^T (\boldsymbol{y}^{+i}(t) - \boldsymbol{y}^{-i}(t))^T(\boldsymbol{y}^{+j}(t) - \boldsymbol{y}^{-j}(t))dt. \tag{4.4}$$

as previously described. Finally, we will make the following definition,

$$\hat{\boldsymbol{P}}(T,\boldsymbol{x}^0)_{i,j} = \frac{1}{4\epsilon^2}\int_0^T \underbrace{(\boldsymbol{y}^{+i}(t) - \boldsymbol{y}^{-i}(t))'}_{\boldsymbol{d}_i}\underbrace{(\boldsymbol{y}^{+j}(t) - \boldsymbol{y}^{-j}(t))}_{\boldsymbol{d}_j}dt. \tag{4.5}$$

From that definition we define $\boldsymbol{d}$ for each of the three state perturbations,

$$\begin{aligned} \boldsymbol{x}^0 \pm \epsilon\boldsymbol{e}_1 \rightarrow \boldsymbol{d}_1 = \boldsymbol{y}^{+1} - \boldsymbol{y}^{-1} &= \begin{bmatrix} 0 \\ (x_1^{+1}(t) + x_2(t))^2 - (x_1^{-1}(t) + x_2(t))^2 \end{bmatrix} \\ \boldsymbol{x}^0 \pm \epsilon\boldsymbol{e}_2 \rightarrow \boldsymbol{d}_2 = \boldsymbol{y}^{+2} - \boldsymbol{y}^{-2} &= \begin{bmatrix} 0 \\ (x_1(t) + x_2^{+2}(t))^2 - (x_1(t) + x_2^{-2}(t))^2 \end{bmatrix} \\ \boldsymbol{x}^0 \pm \epsilon\boldsymbol{e}_3 \rightarrow \boldsymbol{d}_3 = \boldsymbol{y}^{+3} - \boldsymbol{y}^{-3} &= \begin{bmatrix} x_3^{+3}(t) - x_3^{-3}(t) \\ 0 \end{bmatrix}, \end{aligned} \tag{4.6}$$

which will be used later.

### *4.1.2 Fixed AUV*

Now, when we consider the inverse scenario in which the AUV is fixed at the origin and the CNA is governed by constant speed unicycle dynamics. The state of the AUV relative to the CNA is

$$\boldsymbol{r} = \begin{bmatrix} 0 \\ 0 \\ 0 \end{bmatrix} - \begin{bmatrix} x_E \\ y_N \\ -\psi - 180 \end{bmatrix} = \begin{bmatrix} -x_1 \\ -x_2 \\ x_3 + 180 \end{bmatrix}. \tag{4.7}$$

Given the previous discussion of localization assumptions, the observation equation for the relative system can be taken as

$$\boldsymbol{y} = \begin{bmatrix} \psi + 180 \\ r_1^2 + r_2^2 \end{bmatrix}. \tag{4.8}$$

Considering an empirical observability gramian for this system we can again define $\boldsymbol{d}$,

$$\begin{aligned} \boldsymbol{r}^0 \pm \epsilon \boldsymbol{e}_1 \to \boldsymbol{d}_1 = \boldsymbol{y}^{+1} - \boldsymbol{y}^{-1} &= \begin{bmatrix} 0 \\ (r_1^{+1}(t) + r_2(t))^2 - (r_1^{-1}(t) + r_2(t))^2 \end{bmatrix} \\ \boldsymbol{r}^0 \pm \epsilon \boldsymbol{e}_2 \to \boldsymbol{d}_2 = \boldsymbol{y}^{+2} - \boldsymbol{y}^{-2} &= \begin{bmatrix} 0 \\ (r_1(t) + r_2^{+2}(t))^2 - (r_1(t) + r_2^{-2}(t))^2 \end{bmatrix} \\ \boldsymbol{r}^0 \pm \epsilon \boldsymbol{e}_3 \to \boldsymbol{d}_3 = \boldsymbol{y}^{+3} - \boldsymbol{y}^{-3} &= \begin{bmatrix} r_3^{+3}(t) - r_3^{-3}(t) \\ 0 \end{bmatrix}. \end{aligned} \tag{4.9}$$

Given the definition of the relative state (4.7), we arrive at an equality of the integrand terms,

$$\begin{bmatrix} 0 \\ (r_1^{+1}(t) + r_2(t))^2 - (r_1^{-1}(t) + r_2(t))^2 \end{bmatrix} = \begin{bmatrix} 0 \\ (-x_1^{+1}(t) + -x_2(t))^2 - (-x_1^{-1}(t) + -x_2(t))^2 \end{bmatrix}$$
$$\begin{bmatrix} 0 \\ (r_1(t) + r_2^{+2}(t))^2 - (r_1(t) + r_2^{-2}(t))^2 \end{bmatrix} = \begin{bmatrix} 0 \\ (-x_1(t) + -x_2^{+2}(t))^2 - (-x_1(t) + -x_2^{-2}(t))^2 \end{bmatrix}$$
$$\begin{bmatrix} r_3^{+3}(t) - r_3^{-3}(t) \\ 0 \end{bmatrix} = \begin{bmatrix} x_3^{+3}(t) + 180 - (x_3^{-3}(t) + 180) \\ 0 \end{bmatrix}, \tag{4.10}$$

and therefore conclude the systems share the same empirical observability gramian.

### *4.2 Decision Process*

The basic idea of this approach is as follows: Given the current position and orientation of the CNA, determine which of a discrete set of turning angles minimizes the condition number of the empirical local observability gramian. Given a discrete set of turning angles, the CNA can determine the empirical observability gramian that would result from each turn rate, determine the condition number of the empirical gramian, and then select the turn rate that corresponds to the minimum condition number. The decision process can be summarized in an algorithmic form listed as Algorithm 1.

The algorithm can be extended to support multiple AUVs by summing the condition numbers associated with each turn rate for each AUV. We can then select the turn rate that corresponds to the minimum average condition number across the AUVs. The extension of the algorithm to multiple AUVs is given as Algorithm 2.

The pertinent question regarding the decision scheme is what duration of simulation should be used to determine the gramian for each turn rate. Since the simulation assumes a continued application of the same control input, any duration greater than

**Algorithm 1** Single vehicle gramian-based path planning.

**for** each turn rate $u_i$ **do**

  **for** j from 1 to m **do**

    $\breve{\boldsymbol{x}}(n+j+1) \leftarrow$ CNA_Dynamics($\breve{\boldsymbol{x}}(n+j), u_i$)

  **end for**

  $\boldsymbol{P}(u_i) \leftarrow$ empiricalObsvGram($\breve{\boldsymbol{x}}(n)$,...$\breve{\boldsymbol{x}}(n+m)$)

  cNum$_i \leftarrow$ conditionNumber($\boldsymbol{P}(u_i)$)

**end for**

$u^* \leftarrow$ min(cNum)

$\boldsymbol{x}(n+1) \leftarrow$ CNA_Dynamics($\boldsymbol{x}(n), u^*$)

one time step is an approximation. However, using only one time step may not provide enough difference between the trajectories to substantially affect the measurements and the corresponding gramians. In order to move forward with simulation, it was decided that a good trade would consider the minimum turning radius of the vehicle and the vehicle's speed. Given these two values, a propagation time was selected that would take the CNA around two thirds of the circumference of its minimum-radius trajectory. The significance of this duration is that it provides the CNA an ability to account for the effect of moving in any direction from its current location.

**Algorithm 2** Multiple vehicle gramian-based path planning.

**for** each turn rate $u_i$ **do**

  **for** each relative CNA position $\breve{\boldsymbol{x}}_k$ **do**

    **for** j from 1 to m **do**

      $\breve{\boldsymbol{x}}_k(n+j+1) \leftarrow \text{CNA\_Dynamics}(\breve{\boldsymbol{x}}_k(n+j), u_i)$

    **end for**

    $\boldsymbol{P} \leftarrow \text{empiricalObsvGram}(\breve{\boldsymbol{x}}_k(n),...\breve{\boldsymbol{x}}_k(n+m))$

    $\text{cNum}_i \leftarrow \text{cNum}_i + \text{conditionNumber}(\boldsymbol{P})$

  **end for**

**end for**

$u^* \leftarrow \min(\text{cNum})$

$\boldsymbol{x}(n+1) \leftarrow \text{CNA\_Dynamics}(\boldsymbol{x}(n), u^*)$

# Chapter 5
# SIMULATIONS

In the work that follows both path planning methods are tested against various combinations of the number of vehicles involved, the initial conditions of the vehicles, and the control behavior of the AUVs. The CNA is a unit speed vehicle with a minimum turning radius of 0.5 meters.

## *5.1 Path Intertia Method*

### *5.1.1 Single, Fixed AUV*

As a first check of the behavior of the path inertia method, the CNA is placed in a similar initial condition to that used for simulation of an analytic solution in [11]. The analytic solution is a circular path centered on the AUV. As seen in Fig. 5.1 the resulting path agrees with the analytic solution. We also see that the instantaneous estimation condition number resulting from the predicted path remains fixed at its minimum value, one.

A Monte Carlo approach was taken in trying to determine a typical result for the method. Using randomized initial conditions for the CNA vehicle, 50 simulations were executed. The resulting paths suggest that the CNA behavior will fall into one of three categories. First, if the CNA's initial heading makes an obtuse angle with the ray connecting the CNA and AUV, the CNA will steadily spiral outward from the AUV. Second, if the initial heading is at a right angle with the connecting ray, the CNA will proceed to circle the AUV with a radius equal to the length of the connecting ray. Finally, if the initial heading is acute with the connecting ray, the CNA will "fall" toward the AUV. After passing through or near the AUV, the angle will be

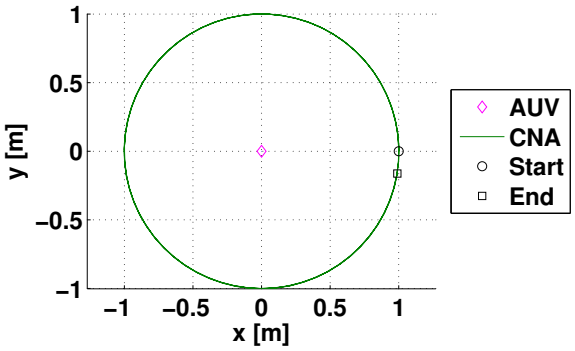


(a) The spatial trajectory of the CNA.

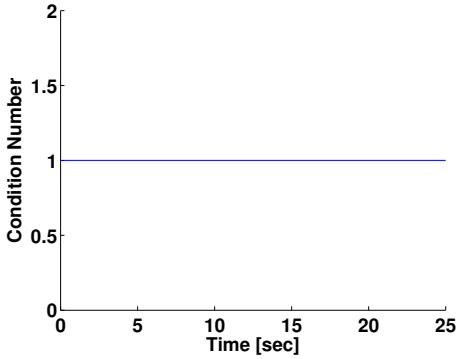


(b) The instantaneous estimation condition number.

Figure 5.1: A CNA path generated with the path inertia method. The CNA starts at (1,0), heading in the $+y$ direction. The AUV remains static at the origin.

obtuse and the CNA will begin an outward spiral motion. Trajectories representative of the three categories are depicted in Fig. 5.2. For completeness, the trajectories resulting from the Monte Carlo experiment are presented in Fig. 5.3 along with a trace of the distance between the CNA and the AUV for each simulation. Note that in every simulation if the distance is initially increasing, it will continue to increase monotonically. However, if the distance is initially decreasing, it will decrease to zero, or very near zero, after which it will monotonically increase.

From the results of the Monte Carlo experiment we see that the decision method is not of much use when we recall that for communication purposes the AUV and CNA should be closer rather than farther apart. After modifying the decision process to use the cost function of (3.24), we go back to comparing the new process to the analytic solution, as was done for the original process in Fig. 5.1. We find, as depicted in Fig. 5.4, that the new process does not produce behavior consistent with the analytic result of [11]. Despite the disagreement, the behavior is at least consistent with our expectations of a plan that considers a cost for the distance between the vehicles in

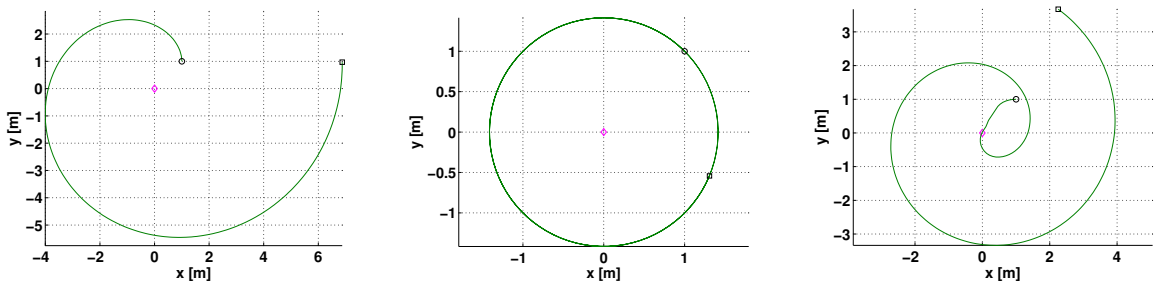


(a) Result of an obtuse initial angle.

(b) Result of a right initial angle.

(c) Result of an acute initial angle.

Figure 5.2: Demonstration of typical paths resulting from path inertia method.

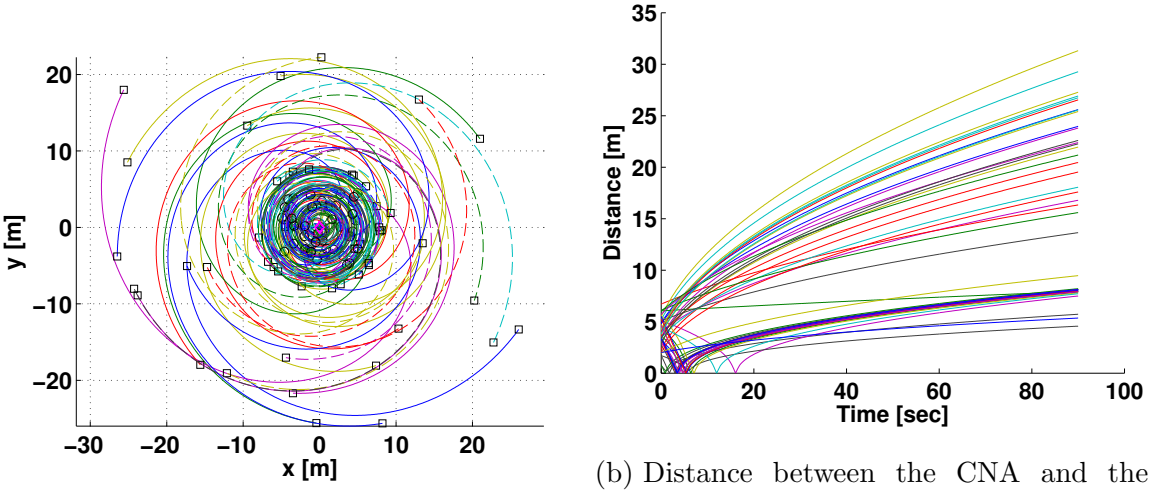


(a) Spatial trajectories of the CNA.

(b) Distance between the CNA and the AUV.

Figure 5.3: Monte Carlo experiment of 50 simulations of the path inertia method.

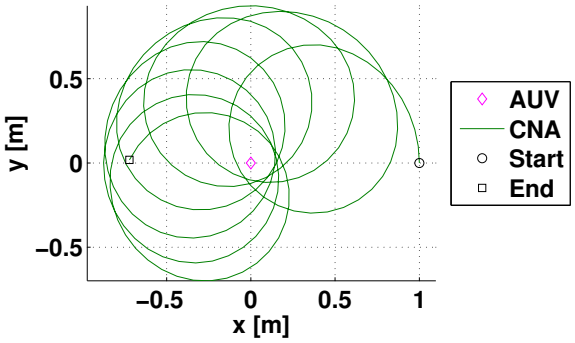


(a) The spatial trajectory of the CNA.

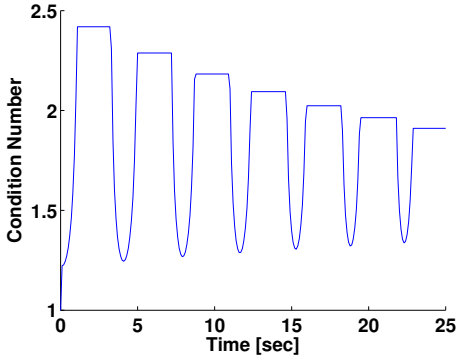


(b) The instantaneous estimation condition number.

Figure 5.4: CNA path generated with modified path inertia method ($\gamma = 1$). The CNA starts at (1,0), heading in the $+y$ direction. The AUV remains static at the origin.

that the CNA is, on average, closer to the AUV than it was in Fig. 5.1.

From another Monte Carlo experiment we find that the behavior of the trajectories from the modified decision process fall into one of two categories that are again distinguished by the angle the CNA heading makes with the ray connecting the CNA and AUV. If the angle is obtuse, the CNA will encircle the AUV with an initial period of increasing separation but which is followed by decreasing separation and settles into a nearly steady, pivoting orbit around the AUV. If the original angle is right or acute, the CNA forgoes the initial increasing separation period but is otherwise the same as the first category of trajectories. The two types of behavior described are depicted in Fig. 5.5. It should be noted that the smallest curves are determined by the minimum turning radius of the CNA (set to 0.5 meters for all simulations). Again, for completeness, we present the result of the Monte Carlo experiment for the modified method in Fig. 5.6. Note that all but one trajectory completely demonstrates behavior according to the two-category description. The

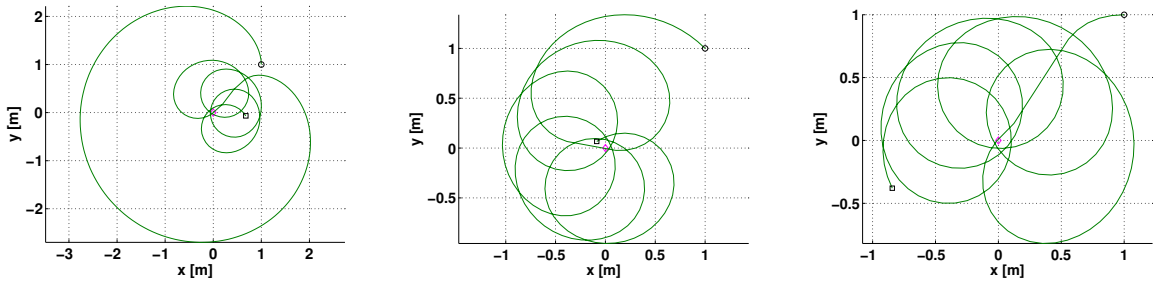


(a) Result of an obtuse initial angle.

(b) Result of a right initial angle.

(c) Result of an acute initial angle.

Figure 5.5: Demonstration of typical paths resulting from modified path inertia method ($\gamma = 1$).

single outlier appears to be consistent with the two-category description but simply wasn't given enough time to complete its approach to the AUV.

Experiments concerned with the value of $\gamma$ were conducted and the trajectories produced exhibited the same two-category behavior. To preserve clarity of the trajectories, the simulations in Fig. 5.7 only show one CNA simulation but are representative of the behavior observed. As depicted in Fig. 5.7, very small values of $\gamma$ permit seemingly indefinite periods of increasing separation. This is expected because a zero value would result in the original decision process. For low values of $\gamma$, in this case between 0.1 and 1.0, the trajectories demonstrate comparatively large periods of increasing separation. However, the trend of simulated paths indicates larger values of $\gamma$ shorten the duration of increasing separation.

### *5.1.2 Multiple AUVs*

Toward a more general goal, we investigate the paths that the decision process yields when there are multiple AUVs for the CNA to tend. Due to the equal consideration of each AUV in (3.26), we suspect that the behavior resulting when multiple AUVs

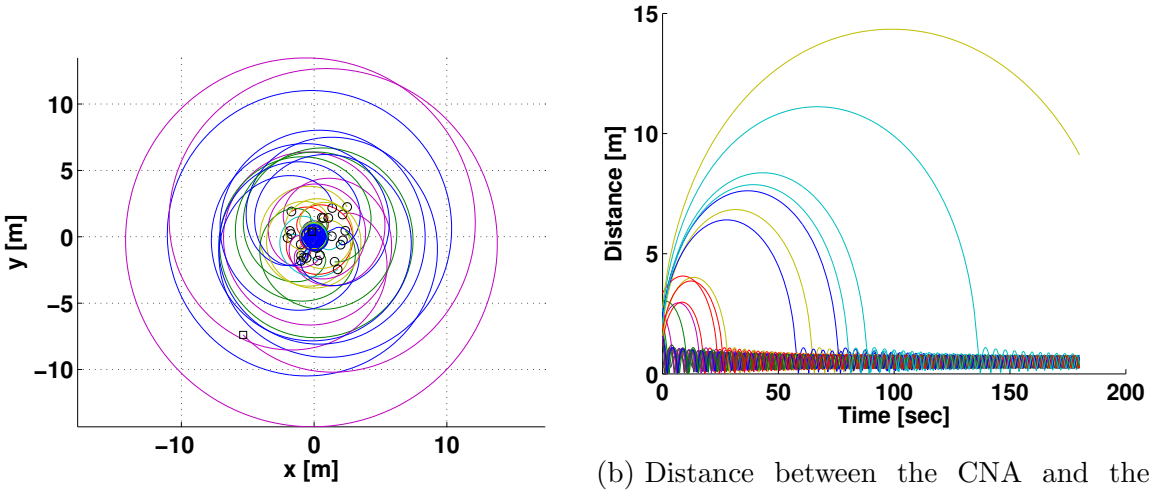


(a) The spatial trajectories of the CNA.

(b) Distance between the CNA and the AUV.

Figure 5.6: Monte Carlo experiment of 25 simulations of the modified path inertia method ($\gamma = 1$).

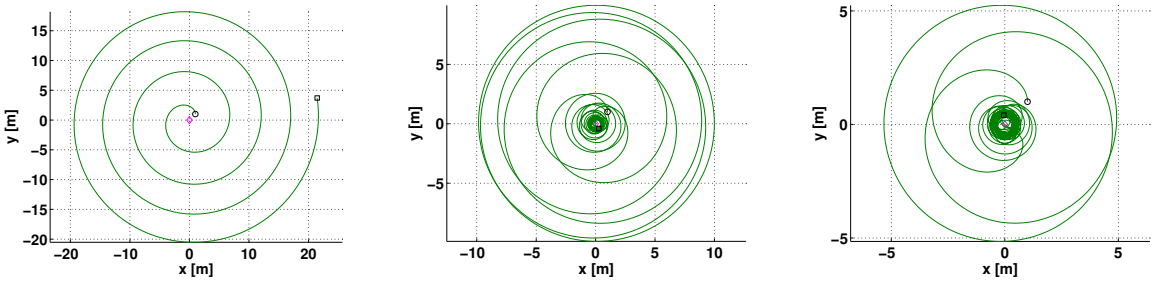


(a) Path generated with $\gamma = 0.01$.

(b) Path generated with $\gamma = 0.10$.

(c) Path generated with $\gamma = 0.25$.

Figure 5.7: Demonstration of the path traits attributed to the variation of $\gamma$.

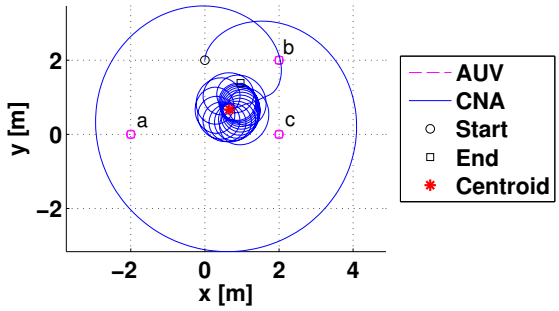


(a) The spatial trajectory of the CNA.

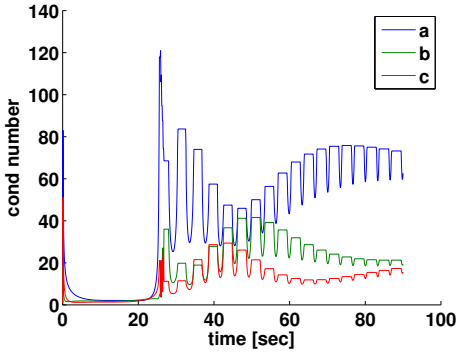


(b) The instantaneous estimation condition numbers.

Figure 5.8: CNA path generated with path modified inertia method ($\gamma = 1$) and a static formation of AUVs. The CNA starts at (0,2), heading in the $+y$ direction.

are present will be similar to that seen before, but without favoring any particular AUV. This suspicion is supported, though it cannot be entirely confirmed, by the simulations conducted. The result of one such simulation can be seen in Fig. 5.8 where the AUVs are arranged in a triangular formation. Note that while the spacial behavior does not appear to favor any one of the AUVs, the estimation condition number approximations suggest that lower-right AUV receives the most desirable performance. In other words, this simulation demonstrates that for this method, equal weighting among vehicles in a group cost function does not imply equal performance from the resulting solution.

At this point we would surmise that the previous results suggest if the formation was mobile, the CNA would continue its categorically described behavior but while in pursuit of centering that behavior on the formation centroid. This hypothesis is also supported by the simulations conducted. For example, we see in Fig. 5.9 that the CNA does the expected thing when the formation moves vertically and then turns

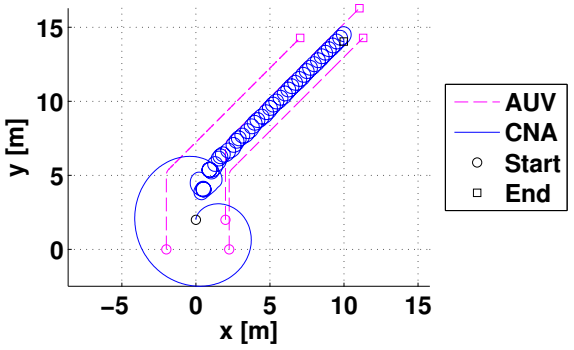


(a) The spatial trajectory of the CNA.

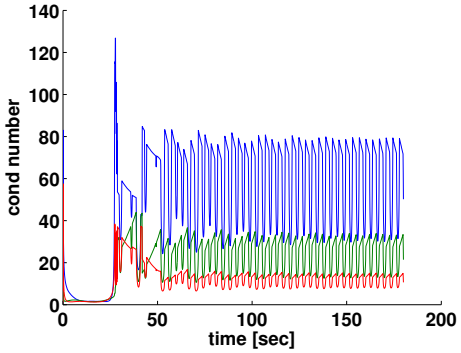


(b) The instantaneous estimation condition number.

Figure 5.9: CNA path generated with path modified inertia method ($\gamma = 1$) and a mobile formation of AUVs. The CNA starts at (0,2), heading in the $+y$ direction.

45° to the right. During the first stage of the simulation the CNA begins its typical behavior centered on the formation centroid. After the formation turns its direction of translation the CNA clearly tracks the formation centroid in the new direction.

In summary, we have seen that toward the limit of very large $\gamma$, the decision process can be replaced with a centroid following/orbiting algorithm, while in the limit of $\gamma$ going to zero we find the CNA spiraling outward from the AUV group centroid. We suppose then that utility of the decision process lies in the middle range of $\gamma$ values where the trajectory may be an improvement over a centroid-orbiting control law.

## *5.2 Empirical Gramian Method*

### *5.2.1 Single AUV*

Starting again with a check against the analytic solution, we see in Fig. 5.10 that the empirical gramian method tends to agree with the analytic circular trajectory. While

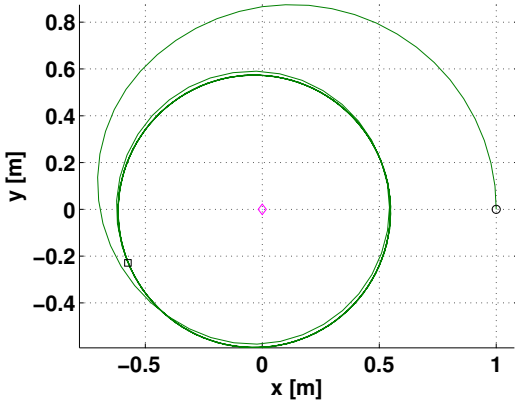


(a) The spatial trajectory of the CNA.

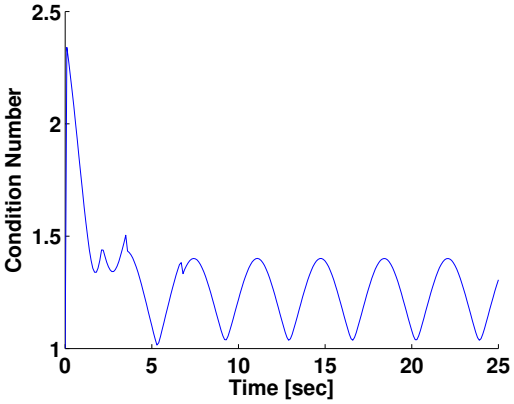


(b) The instantaneous estimation condition number.

Figure 5.10: A CNA path generated with the empirical gramian method. The CNA starts at (1,0), heading in the $+y$ direction. The AUV remains static at the origin.

the first part of the path is a convergent spiral, the remainder demonstrates a circular behavior nearly centered on the AUV. A Monte Carlo experiment of 50 CNAs having randomly selected initial conditions, Fig 5.11, suggests that the convergent spiral behavior is typical of the paths generated by this method. As compared to the path inertia method, we see that there does not seem to be an association between the initial condition of the CNA and resulting path behavior. We also note that the experiment revealed one case in which the CNA did not conform to the typical behavior, indicating there may be some region of initial conditions that produce atypical behavior.

### *5.2.2 Multiple AUVs*

When multiple AUVs are included the behavior the method appears less predictable than that of the path inertia method. As seen in Fig. 5.12, the gramian method does not necessarily converge to a circular trajectory of smallest possible radius, nor

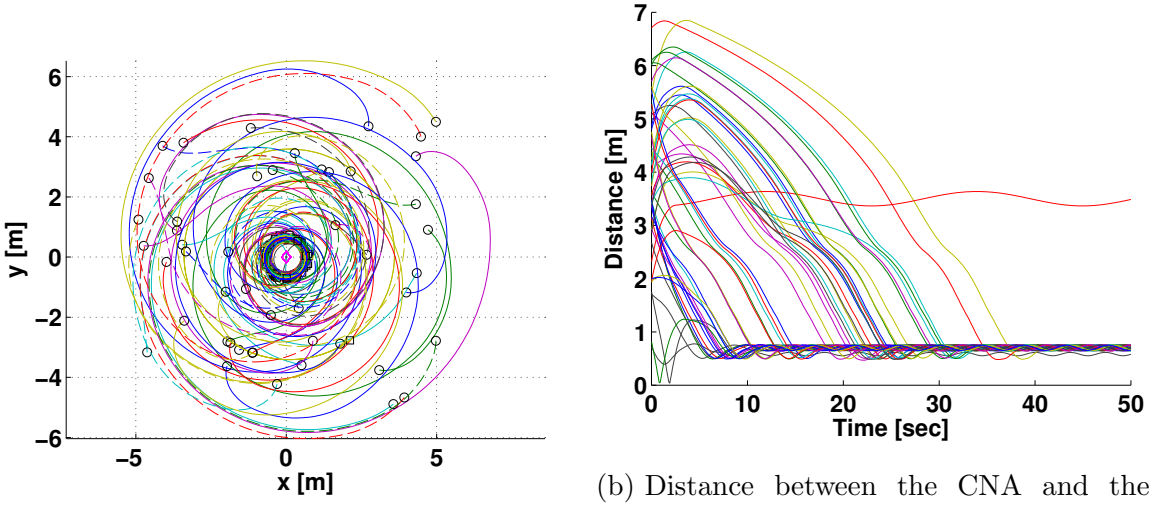


(a) The spatial trajectories of the CNA.

(b) Distance between the CNA and the AUV.

Figure 5.11: Monte Carlo experiment of 50 simulations of the path inertia method.

does it necessarily act about the centroid of the AUV formation. One behavior the simulations have not produced is an indefinitly increasing separation between the CNA and its AUVs. This may be an indication that the empirical gramian method encourages closeness to the AUVs even though such a desire was never explicitly incorporated.

### *5.3 Localization Performance*

A final round of simulations were conducted with the goal of obtaining a notion of the ability of the path planning methods to improve AUV localization accuracy. The scenario considered is a single AUV conducting a lawnmower survey pattern. For comparison, simulations were conducted in which the CNA remained stationary and in which the CNA traversed a large circular trajectory that encompasses the survey area. In order to simulate estimation performance, the AUV is employing and Extended Kalman Filter (EKF) to estimate its planar position, heading, and

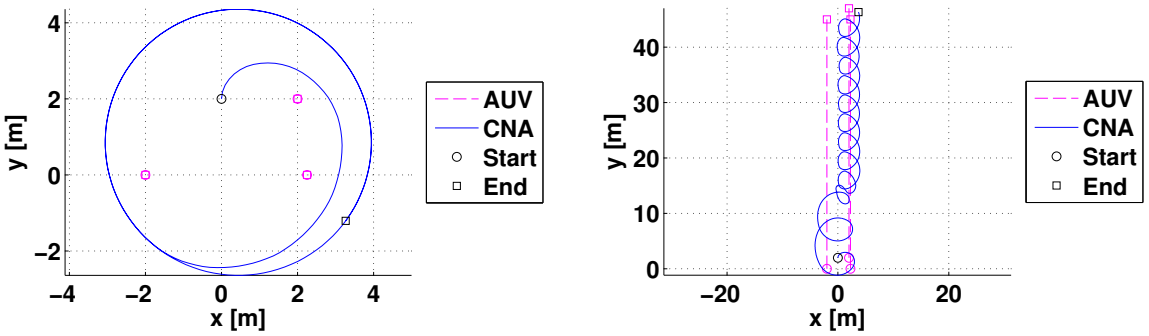


(a) The spatial trajectory of a CNA with a static AUV formation.

(b) The spatial trajectory of a CNA with a mobile AUV formation.

Figure 5.12: Trajectories resulting from the empirical gramian method when multiple AUVs are serviced.

velocity. The system in (4.1) is used as the model in the EKF. In all simulations the AUV assumes the same values for process and measurement noise variance, and in all simulations respective samples are affected by an identical, pre-determined, vector of noise values. Thus, the CNA path is the only differing aspect between the simulations. In all cases, the initial position of the AUV is (-2,0) and the initial estimate is set to (0,0).

In the first experiment, the CNA is considered "fast", meaning that it moves 10 times faster than the AUV. Table 5.1 summarizes the results of the associated simulations. Depictions of the paths and estimation performance can be found in Appendix B. Note that the smallest possible maximum distance error is 2 m, because of the discrepancy between the AUV's initial position and its initial estimate. From Table 5.1 we see that both planning methods dramatically out-perform the stationary and large circular CNA paths. With the CNA able to move so much faster than the AUV the behavior of both planning methods provided a number of encirclements of the CNA about the AUV as the AUV moved along its path.

Table 5.1: Localization performance results with fast CNA.

| | Distance Error [m] | |
|---|---|---|
| Method | RMS | Max |
| Empirical Gramian | 0.1 | 2.3 |
| Path Inertia ($\gamma = 1$) | 0.2 | 3.1 |
| Circular | 29.3 | 117.8 |
| Stationary | 71.0 | 118.0 |

In the second experiment, the CNA is considered "slow", meaning the CNA and the AUV travel at the same speed. Table 5.2 summarizes the results of those simulations. Again, depictions of the paths and estimation performance can be found in Appendix B. From Table 5.2 we note that the results are mixed from the fast case. While the path inertia method achieved nearly identical performance, the empirical gramian method showed a marked performance reduction. The combination of these experiments suggest that the planning methods carry some utility in improving AUV localization performance. However, they also suggest that the method bearing the most utility may be dependent on the AUV mission and the speeds of the vehicles.

Table 5.2: Localization performance results with slow CNA.

| | Distance Error [m] | |
|---|---|---|
| Method | RMS | Max |
| Path Inertia ($\gamma = 1$) | 0.3 | 3.1 |
| Stationary | 2.5 | 12.6 |
| Empirical Gramian | 5.6 | 16.3 |
| Circular | 24.1 | 48.6 |

# Chapter 6

# CONCLUSION

Inspired by the long term vision proposed by researchers at the Woods Hole Oceanographic Institution, we have presented two alternative decision methods to plan CNA paths aimed at improving the quality of communication and navigation assistance provided by a CNA. While there exist other methods previously developed to improve localization performance in single beacon navigation, the methods developed here were based on improving the conditioning of any estimation scheme an AUV may employ.

In simulations involving the path inertia method, we found that the resulting paths could be characterized based on the initial conditions of the AUV and CNA. We also found that a distance penalty would be necessary in most cases to discourage unbounded separation of the vehicles that the nominal method tends to generate. When testing against multiple AUVs we found that the trajectory behavior was again predictable and demonstrates a tendency to act about the centroid of the AUV group.

Simulations involving the empirical gramian method demonstrated path behavior that was not so readily characterized. While paths typically showed a tight orbiting trend, simulations showed the typical description was not accurate for all cases. Though the process of simulating various scenarios it was experienced that the empirical gramian method can be somewhat sensitive to the duration of simulation used to test possible steering angles.

The final experiments conducted demonstrated that the planning methods can improve estimation accuracy, but their efficacy may depend heavily on the AUV missions used and/or the difference in vehicle speeds. Investigating certain missions

or combinations of vehicle speeds that lead to poor estimation performance, even with the planning methods, could be useful in the design of survey missions and vehicle capabilities.

There are avenues for future work with regard to both planning methods. In the path inertia method there may be interest in applying unequal weight to the terms of the cost function when dealing with multiple AUVs. This weighting could be dynamic to allow emphasis on different vehicles over time. In the empirical gramian method there may be interest in exploring the trade-off between forward simulation accuracy and duration of simulation applied to each turn rate. Also, when multiple AUVs are included, rather than taking the minimum average condition number to decide a steering control, one could use some other measure of aggregate condition number. For example, one could use the minimum RMS condition number or maybe decide by the minimum max value.

Finally, recall that the unobservability index was provided as a measure of estimation sensitivity to measurement noise. For the decision methods developed in this work the estimation condition number was the primary measure of concern. In future work a decision method that considers a combination of the two measures may yield different, possibly better, CNA paths than those seen herein.

# BIBLIOGRAPHY

[1] H. Stommel, "The slocum mission," *Oceanography*, vol. 2, no. 1, pp. 22–25, 1989.

[2] C. Eriksen, T. Osse, R. Light, T. Wen, T. Lehman, P. Sabin, J. Ballard, and A. Chiodi, "Seaglider: a long-range autonomous underwater vehicle for oceanographic research," *Oceanic Engineering, IEEE Journal of*, vol. 26, no. 4, pp. 424–436, 2001.

[3] C. German, M. Jakuba, J. Kinsey, J. Partan, S. Suman, A. Belani, and D. Yoerger, "A long term vision for long-range ship-free deep ocean operations: Persistent presence through coordination of autonomous surface vehicles and autonomous underwater vehicles," in *Autonomous Underwater Vehicles (AUV), 2012 IEEE/OES*, 2012, pp. 1–7.

[4] A. Bahr, "Cooperative localization for autonomous underwater vehicles," Ph.D. dissertation, Massachusetts Institute of Technology Woods Hole Oceanographic Institution, February 2009.

[5] L. Freitag, M. Grund, S. Singh, J. Partan, P. Koski, and K. Ball, "The whoi micro-modem: an acoustic communications and navigation system for multiple platforms," in *OCEANS, 2005. Proceedings of MTS/IEEE*, 2005, pp. 1086–1092 Vol. 2.

[6] P. Baccou and B. Jouvencel, "Homing and navigation using one transponder for auv, postprocessing comparisons results with long base-line navigation," in *Robotics and Automation, 2002. Proceedings. ICRA '02. IEEE International Conference on*, vol. 4, 2002, pp. 4004–4009 vol.4.

[7] B. Ferreira, A. Matos, and N. Cruz, "Single beacon navigation: Localization and control of the mares auv," in *OCEANS 2010*, 2010, pp. 1–9.

[8] M. Larsen, "Synthetic long baseline navigation of underwater vehicles," in *OCEANS 2000 MTS/IEEE Conference and Exhibition*, vol. 3, 2000, pp. 2043–2050 vol.3.

[9] G. Rui and M. Chitre, "Cooperative positioning using range-only measurements between two auvs," in *OCEANS 2010 IEEE - Sydney*, 2010, pp. 1–6.

[10] T.-L. Song, "Observability of target tracking with range-only measurements," *Oceanic Engineering, IEEE Journal of*, vol. 24, no. 3, pp. 383–387, 1999.

[11] B. T. Hinson, M. K. Binder, and K. A. Morgansen, "Path planning to optimize observability in a planar uniform flow field," in *American Control Conference, 2013*, 2013, accepted, not yet published.

[12] A. Gadre and D. Stilwell, "A complete solution to underwater navigation in the presence of unknown currents based on range measurements from a single location," in *Intelligent Robots and Systems, 2005. (IROS 2005). 2005 IEEE/RSJ International Conference on*, 2005, pp. 1420–1425.

[13] P. Batista, C. Silvestre, and P. Oliveira, "Single range aided navigation and source localization: Observability and filter design," *Systems & Control Letters*, vol. 60, no. 8, pp. 665 – 673, 2011. [Online]. Available: http://www.sciencedirect.com/science/article/pii/S0167691111001174

[14] F. Arrichiello, G. Antonelli, A. Aguiar, and A. Pascoal, "Observability metric for the relative localization of auvs based on range and depth measurements: Theory and experiments," in *Intelligent Robots and Systems (IROS), 2011 IEEE/RSJ International Conference on*, 2011, pp. 3166–3171.

[15] G. Papadopoulos, M. Fallon, J. Leonard, and N. Patrikalakis, "Cooperative localization of marine vehicles using nonlinear state estimation," in *Intelligent Robots and Systems (IROS), 2010 IEEE/RSJ International Conference on*, 2010, pp. 4874–4879.

[16] M. Chitre, "Path planning for cooperative underwater range-only navigation using a single beacon," in *Autonomous and Intelligent Systems (AIS), 2010 International Conference on*, 2010, pp. 1–6.

[17] H. J. S. Feder, J. J. Leonard, and C. M. Smith, "Adaptive mobile robot navigation and mapping," *The International Journal of Robotics Research*, vol. 18, no. 7, pp. 650–668, 1999. [Online]. Available: http://ijr.sagepub.com/content/18/7/650.abstract

[18] T. Y. Teck and M. Chitre, "Single beacon cooperative path planning using cross-entropy method," in *OCEANS 2011*, 2011, pp. 1–6.

[19] C.-T. Chen, *Linear System Theory and Design*, 3rd ed. New York, NY, USA: Oxford University Press, Inc., 1998.

[20] A. J. Krener and K. Ide, "Measures of unobservability," in *Decision and Control, 2009 held jointly with the 2009 28th Chinese Control Conference. CDC/CCC 2009. Proceedings of the 48th IEEE Conference on*, 2009, pp. 6401–6406.

# Appendix A

# ACOUSTIC LOCALIZATION METHODS

**USBL** Ultra-Short Baseline Localization is a method typically used when a manned surface vehicle is tending to one or more AUVs operating relatively close to the surface vessel (generally within a few hundred meters). In this method the surface craft sends a ping to the AUV to which the AUV replies. The surface craft receives the response via an array of hydrophones of known spacing and arrangement. Using the travel time of the ping the surface craft can determine the range to the AUV. Using the phase difference of the response signal between the hydrophones the surface craft can determine the bearing toward the AUV. In some implementations the roles are reversed and the AUV has the array (which is more easily scaled to support multiple AUVs). The USBL method is advantageous because a position estimate can be constructed from a single measurement and only requires one beacon which may be a mobile surface craft.

**SBL** Short Baseline Localization is also a method typically used when a manned surface craft is tending one or more AUVs which operate within a relatively close range. In SBL, two or more transponders are typically cast over the sides or ends of a surface vessel with a known location for both transponders. The AUV can then measure the distance from itself to both or all of the transponders to determine its own position. Variations on SBL come from how the range measurement is made, specifically, whether the AUV must converse with each transponder or whether the transponders ping and broadcast their positions on a set schedule (requiring time synchronization throughout the system).

**LBL** Long Baseline Localization is a method typically used when the AUV is to operate over a larger range (on the order of kilometers) and the need for position accuracy warrants the setup/installation of multiple acoustic beacons. In LBL, two or more beacons are fixed at known locations. The distances measured to multiple beacons are combined to form an estimate of the vehicle location with, for example, a nonlinear least squares estimation scheme. A birds-eye-view depiction of an LBL system is given in Fig. A.1. In such a scheme, the surface vehicles supporting the beacons would have access to GPS, and can acoustically communicate their position to the vehicle when necessary.

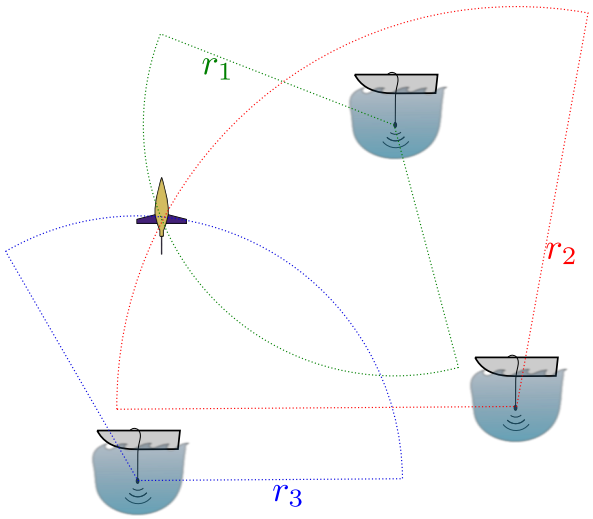


Figure A.1: A birds-eye-view depiction of a long baseline localization system.

**MLBL** Moving Long Baseline Localization in its simplest form has already been depicted in the LBL case. By some definitions an LBL scheme requires the beacons to be *absolutely* fixed. In the LBL scheme depicted, the beacons can be mobile so long as the vehicle can obtain the beacon's location at the time of a ping response. Because the beacons are allowed to move, the scheme can be considered a case of MLBL. However, another scheme is one in which a single

beacon is involved and the vehicle must estimate the postion of the beacon by taking spatially separated measurements, as in Fig. A.2. This form of the MLBL scheme is commonly reffered to as single beacon navigation (SBN). In this scenario, an estimation scheme that incorporates the AUV's dynamics must be used to create a position estimate. An assortment of prior works have been focused on the development and implementation of estimation schemes for SBN.

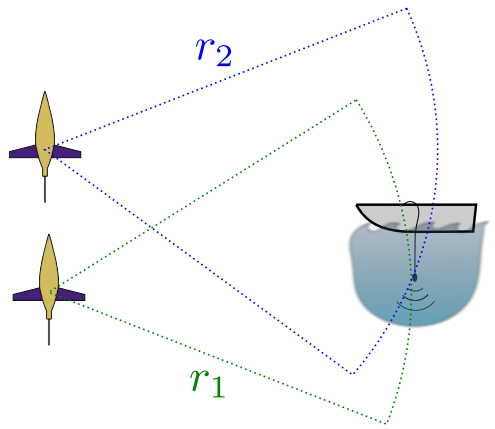


Figure A.2: A birds-eye-view depiction of a moving long baseline localization system.

# Appendix B

# ESTIMATION PERFORMANCE SIMULATIONS

This appendix provides depictions of the simulation results in which an AUV follows a typical survey path while maintaining an estimate of its position. In all cases the AUV is estimating position with an Extended Kalman Filter (EKF). The initial position of the AUV is always (-2,0) while the initial guess provided to the EKF is (0,0). In addition to simulating estimation performance of paths made by planning, a large circular CNA path and a stationary CNA are simulated for comparison.

## *B.1 "Slow" CNA Simulations*

This section provides depictions of the simulation results from cases when the both the AUV and CNA travel at 1 m/s. From Fig. B.1 we see that the large circular trajectory is placed to encompass a majority of the AUV's survey area. The estimation performance for this scenario is very poor. The large drift in the estimate error can be reasoned by considering the first third of the CNA trajectory. During the segment when the CNA is above the trajectory of the AUV (in the y-direction), vertical motion of the AUV is motion along a straight line that passes through (or near) the location of the beacon. Previous observability analysis has shown that such motions degrade position observability.

The performance of the stationary CNA scenario is entirely dependent on the motion path of the AUV. Despite this restriction, as seen in Fig. B.2, the lawnmower path seems to provide sufficient motion to allow the EKF to lock on to the AUV position.

The path inertia method with a distance cost yields a path that essentially follows

the AUV, see Fig. B.3. We see the $x$ and $y$ estimate uncertainty grow and shrink as the AUV turns from horizontal motion to vertical motion, however the estimation error does not grow accordingly.

From Fig. B.4, we see that the empirical gramian method produces an un-intuitive trajectory. Unfortunately, this simulation suggests that the empirical gramian method may suffer in situations where AUVs are of comparable speed to the CNA.

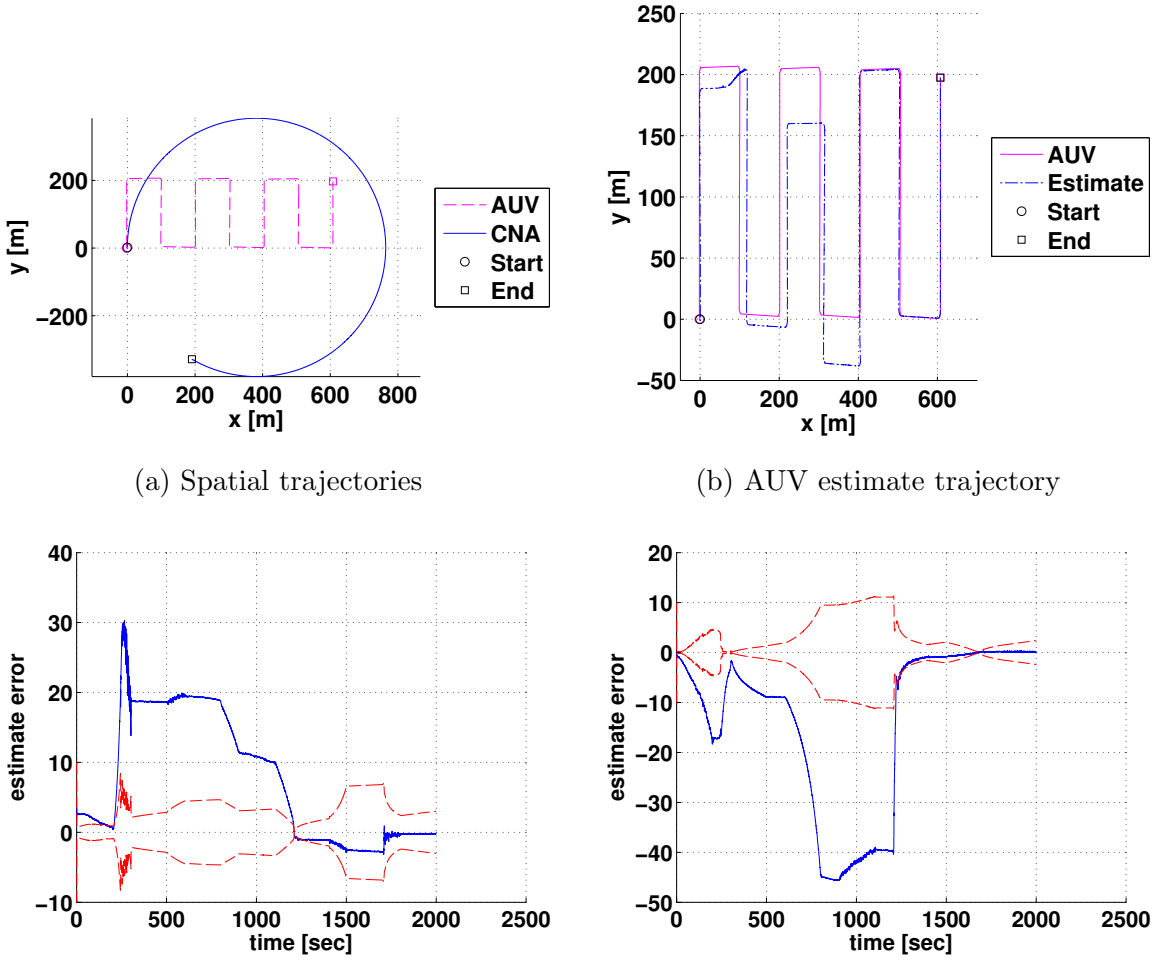


(a) Spatial trajectories

(b) AUV estimate trajectory

(c) $x_E$ estimate error [m]

(d) $y_N$ estimate error [m]

Figure B.1: Slow CNA simulation results for large circular CNA path.

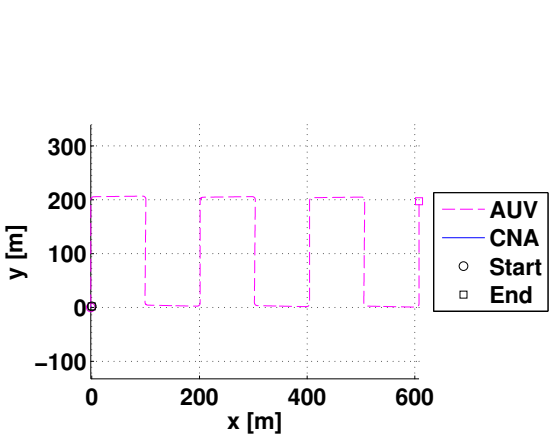


(a) Spatial trajectories

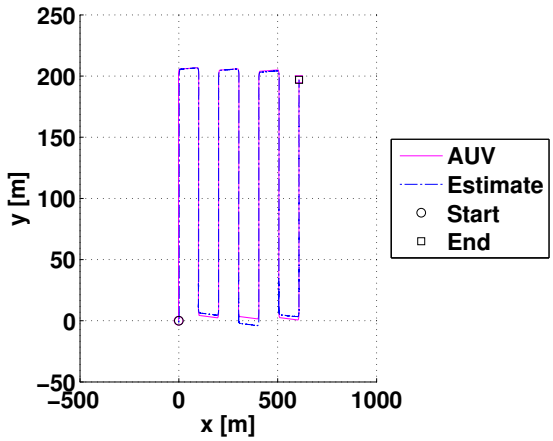


(b) AUV estimate trajectory

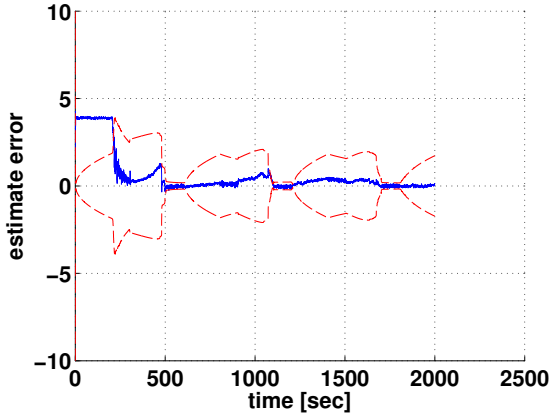


(c) $x_E$ estimate error [m]

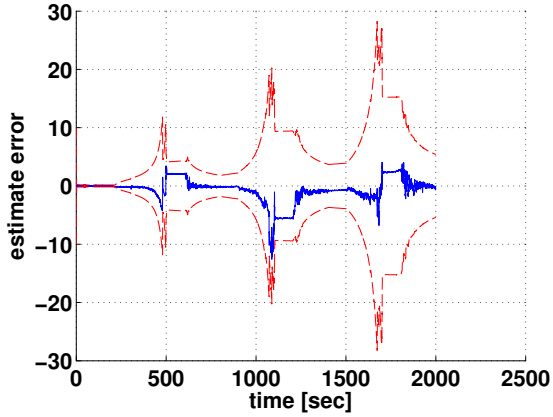


(d) $y_N$ estimate error [m]

Figure B.2: Slow CNA simulation results for stationary CNA.

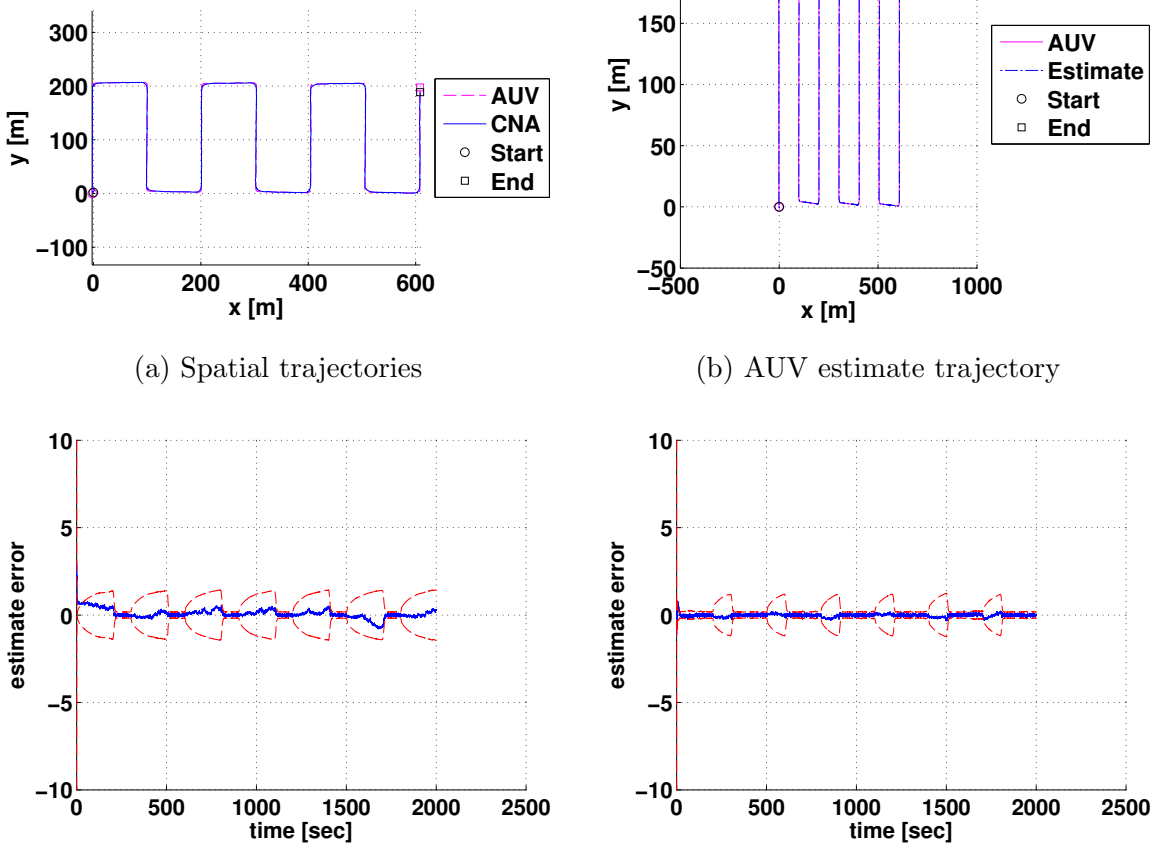


(a) Spatial trajectories

(b) AUV estimate trajectory

(c) $x_E$ estimate error

(d) $y_N$ estimate error

Figure B.3: Slow CNA simulation results for CNA path made by path inertia method ($\gamma = 1$).

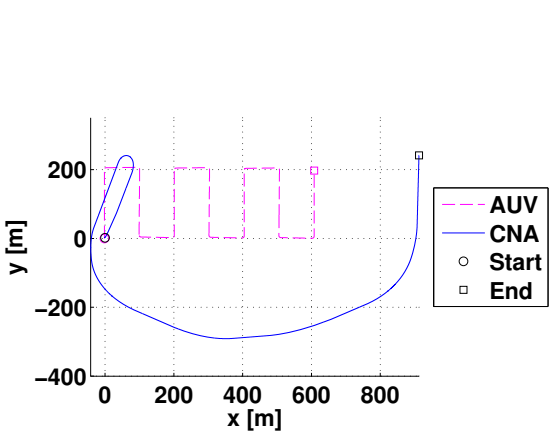


(a) Spatial trajectories

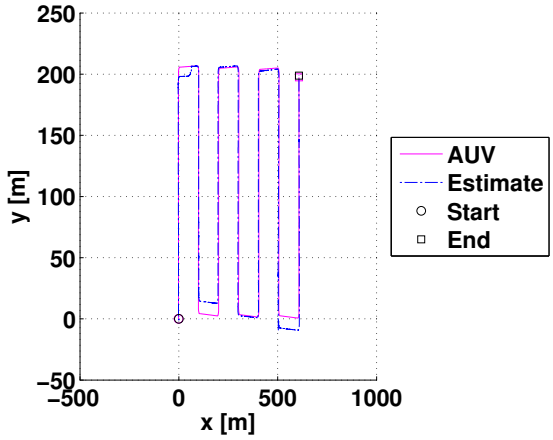


(b) AUV estimate trajectory

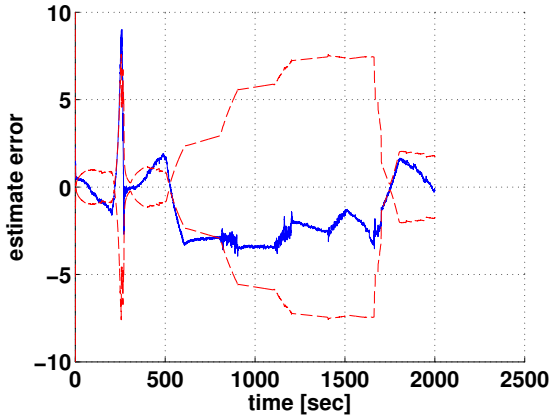


(c) $x_E$ estimate error

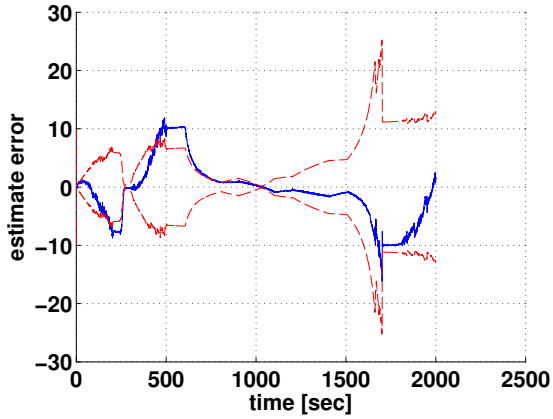


(d) $y_N$ estimate error

Figure B.4: Slow CNA simulation results for CNA path made by empirical gramian method.

### *B.2 "Fast" CNA Simulations*

This section provides depictions of the simulation results from cases when the CNA travels at 1 m/s and the AUV travels at 0.1 m/s. From Fig. B.5 we see that the large circular trajectory is again placed to encompass a majority of the AUV's survey area. The estimation performance for this scenario is again very poor. As opposed to the "slow" case, the estimation error in this simulation are much larger. A likely explanation for this difference is that the AUV is much smaller and given the same initial error in the estimate, a correction of the error could have over inflated the speed estimate (which started at 0 m/s), to cause a large excursion away from the correct estimate.

The performance of the stationary CNA in the fast scenario is much worse than in the slow case. As seen in Fig. B.6, it appears that the EKF locks on to an incorrect estimate which mirrors the actual position over the $y$-axis.

In the fast scenario, the path inertia method again follows the AUV but this time encircling it repeatedly, as seen in Fig. B.7. We see the $x$ and $y$ estimate uncertainty again grow and shrink as the AUV turns from horizontal motion to vertical motion. In this case however, the estimation error does grow slightly in accordance with the uncertainty.

From Fig. B.8, we see that the empirical gramian method produces a similar trajectory to the path inertia method. The estimation error follows the same trend as well; increasing and decreasing in the $x$ and $y$ directions in accordance with horizontal and vertical motion of the AUV.

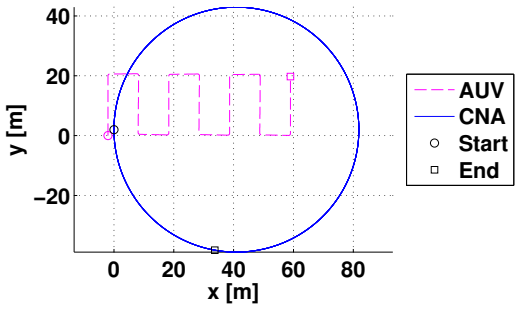


(a) Spatial trajectories

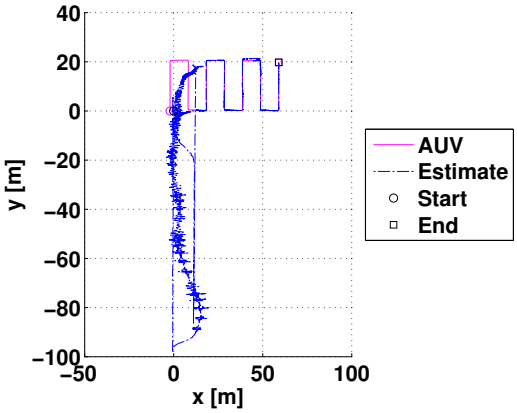


(b) AUV estimate trajectory

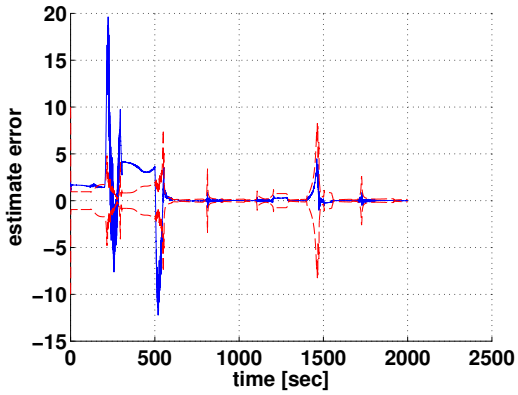


(c) $x_E$ estimate error

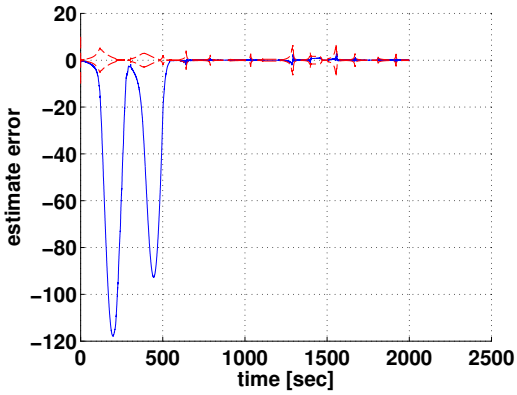


(d) $y_N$ estimate error

Figure B.5: Fast CNA simulation results for large circular CNA path.

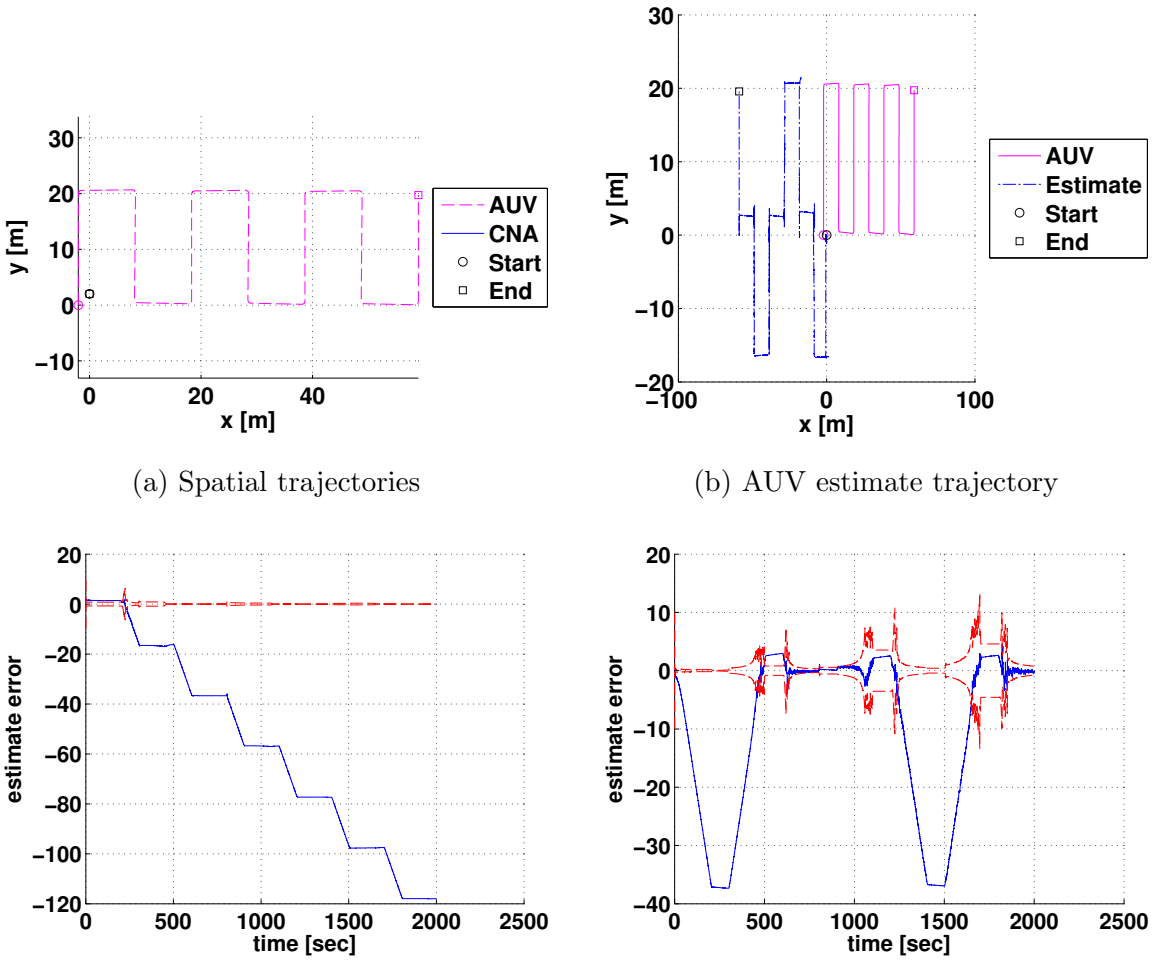


(a) Spatial trajectories

(b) AUV estimate trajectory

(c) $x_E$ estimate error

(d) $y_N$ estimate error

Figure B.6: Fast CNA simulation results for stationary CNA.

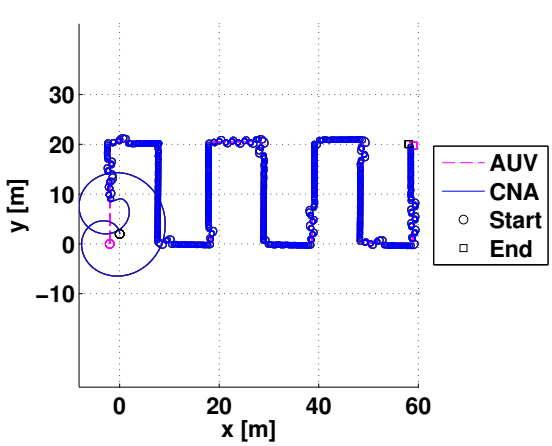


(a) Spatial trajectories

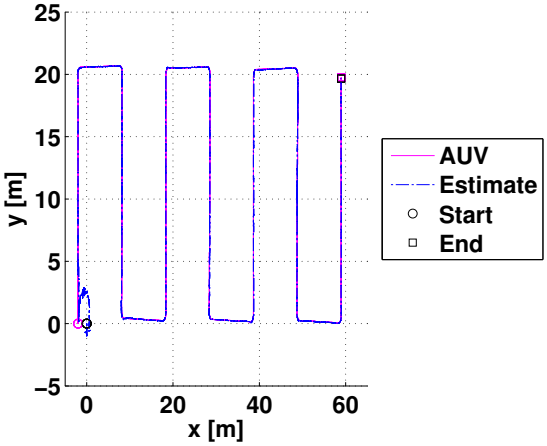


(b) AUV estimate trajectory

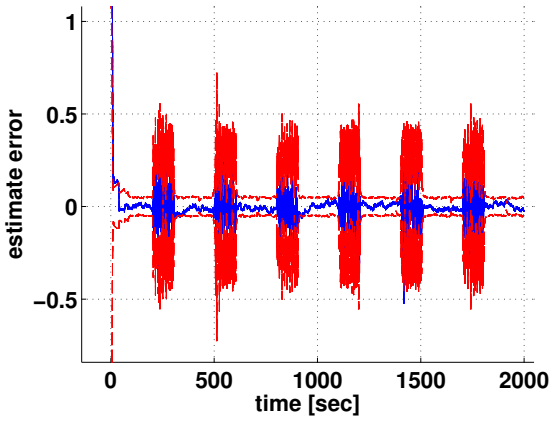


(c) $x_E$ estimate error

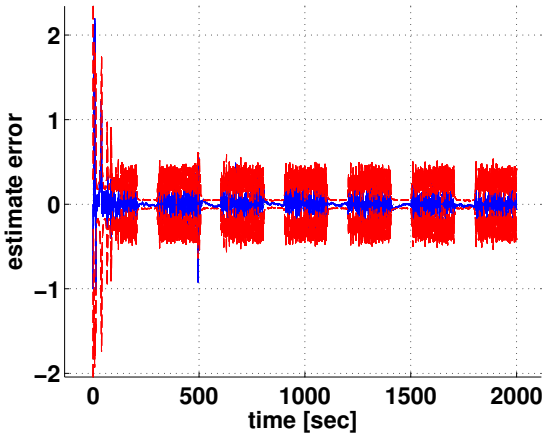


(d) $y_N$ estimate error

Figure B.7: Fast CNA simulation results for CNA path made by path inertia method ($\gamma = 1$).

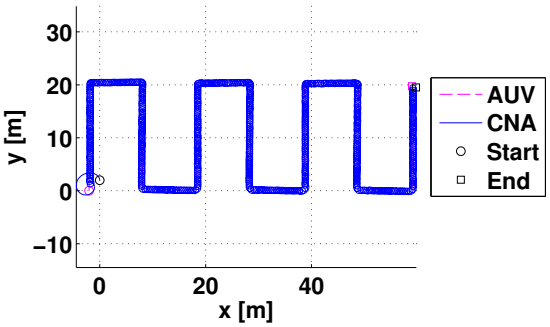


(a) Spatial trajectories

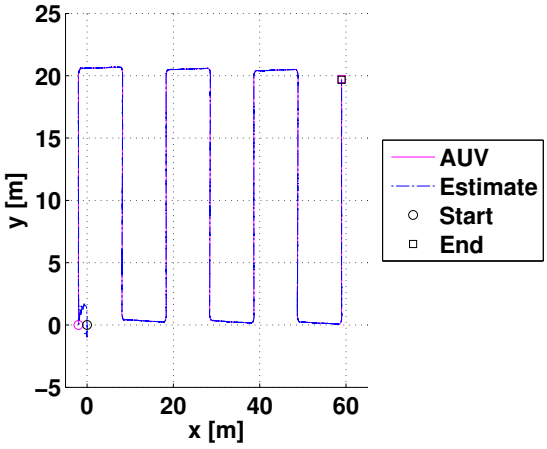


(b) AUV estimate trajectory

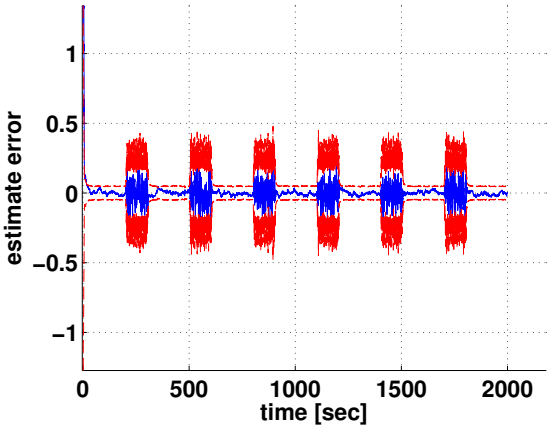


(c) $x_E$ estimate error

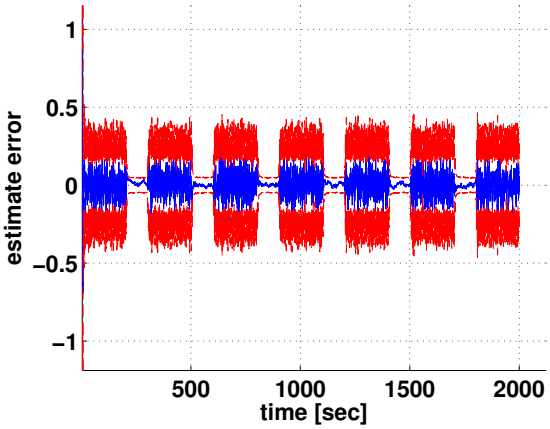


(d) $y_N$ estimate error

Figure B.8: Fast CNA simulation results for CNA path made by empirical gramian method.